Acta Mech
https://doi.org/10.1007/s00707-021-03045-x

ORIGINAL PAPER

**Dario Bettamin · Ahmed A. Shabana · Nicola Bosso · Nicolò Zampieri**

# Frenet force analysis in performance evaluation of railroad vehicle systems

Received: 2 June 2021 / Accepted: 20 June 2021


**Abstract** A *data-driven science* approach, based on integrating nonlinear *multibody system* (MBS) formulations and new geometric concepts, is used in this paper to compare the performance of two widely used railroad bogies: the *three-piece bogie* and the *Y25 bogie*. MBS algorithms are used to solve the bogie nonlinear differential/algebraic equations (DAEs) to determine the bogie motion trajectories. To have a better understanding of the bogie dynamic behavior, a distinction is made between the geometry of *actual motion trajectories* (AMT) and the track geometry. The AMT curves are described using the motion-dependent Frenet–Euler angles, referred to as Frenet bank, curvature, and vertical development angles, which differ from their counterparts used in the description of the track geometry. In particular, the Frenet bank angle defines the super-elevation of the AMT curve *osculating plane*, referred to as the *motion plane*, distinguishing this Frenet super-elevation from the fixed-in-time track super-elevation. The paper explains the difference between the *lateral track plane force balance* used in practice to determine the balance speed and the *Frenet force balance* which is based on recorded motion trajectories. Computer simulations of bogies travelling on a track, consisting of tangent, spiral, and curve sections are performed with particular attention given to the deviations of the AMT curves from the track centerline. The results obtained in this study demonstrate the dependence of the AMT curve geometry on the wheelset forward motion, highlighting the limitations of tests performed using roller test rigs which do not allow longitudinal wheelset motion.

## 1 Introduction

Freight rail transportation is considered more efficient and more environmentally friendly compared to highway transportation [4]. To enhance the performance and safety of rail transportation, railroad vehicle dynamics and stability have been the subject of a large number of investigations [1, 2, 5, 8, 9, 16, 18, 26, 27, 28, 32, 49]. Nonetheless, railroad vehicle derailments, which received special attention, remain common, including derailments resulting from wheel climb at relatively low speeds. Furthermore, derailment criteria failed to provide explanation of many accidents due to several reasons: (i) some derailment criteria are based on

D. Bettamin · A. A. Shabana (✉)
Department of Mechanical and Industrial Engineering, University of Illinois at Chicago,
842 West Taylor Street, Chicago, IL 60607, USA
e-mail: shabana@uic.edu

D. Bettamin
e-mail: s275775@studenti.polito.it

D. Bettamin · N. Bosso · N. Zampieri
Department of Mechanical and Aerospace Engineering, Politecnico di Torino, Turin, Italy
e-mail: nicola.bosso@polito.it

N. Zampieri
e-mail: nicolo.zampieri@polito.it

Published online: 17 August 2021

simplified approaches that do not take into account the three-dimensional nature of the forces that lead to wheel climb; (ii) lack of proper interpretation of the wheelset forces including inertia forces; and (iii) misinterpretation of the role of the track geometry and its influence on the vehicle dynamics. Because of the railroad wheel conicity, the simplest motion of a wheelset is three-dimensional, and consequently, use of three-dimensional force analysis is necessary. Planar force equilibrium can lead to simplifications that ignore the complex nature of the three-dimensional dynamics of the railroad vehicles.

Misinterpretation of the forces that influence the motion of the railroad vehicle is another factor that has contributed to limiting the effectiveness of existing derailment criteria. Even in the case of a tangent (straight) track, the lateral inertia force due to the hunting oscillations can be significant. This lateral force, which can be interpreted as a centrifugal inertia force, can exert high force on the track structure if it is not properly balanced [40]. During hunting oscillations on a tangent track, centers of mass of vehicle components trace space curves that have their own geometric characteristics. Curve motion, regardless of the track geometry, produces centrifugal inertia forces that can have significant lateral component. The magnitude of such a lateral centrifugal force component increases in case of heavier vehicles operating at higher speeds. The actual motion trajectories can be sharp curves with large curvatures and small radii of curvatures, much smaller than the *minimum curve radius* mandated in North America by federal regulations when constructing the track geometry. Recorded motion trajectories obtained from computer simulations can be used effectively to shed light on the behavior of the vehicle.

Another important fact often overlooked in the study of railroad vehicle systems is the role of the *track geometry* and its influence on the motion trajectories. For example, track super-elevations are used to create a lateral component of the gravity force to balance the lateral component of the centrifugal inertia force. This force balance is used to define a *balance speed* recommended for the vehicle safe operation during curve negotiations. In defining the balance speed, it is assumed that the rail car strictly traces a circular curve that lies in a plane parallel to the horizontal plane. Because of this assumption, which is often violated, the centrifugal inertia force is assumed to lie in a plane parallel to the horizontal plane. Nonetheless, observations confirm that the gravity/centrifugal force balance does not always eliminate the lateral motion, and as a consequence, the rail car often slides toward the high and low rails, exerting significant lateral force on the track structure. Clearly, the assumption of a horizontal centrifugal inertia force may be satisfied if the wheel flanges remain in continuous contact with a constant curve section of a rail, which is an undesirable motion scenario because of the possibility of high contact force and wheel climb.

In this paper, a *data-driven science* (DDS) approach that integrates nonlinear *multibody system* (MBS) formulations and new geometric concepts is used to compare the performance of two bogies widely used in North America, Europe, and other parts of the world. These bogies are the *three-piece bogie*, used in North America and other parts of the world, and the European *Y25 bogie*. MBS algorithms are used to automatically construct and numerically solve the bogie nonlinear differential/algebraic equations (DAEs) and record motion trajectories that define the system dynamics [13, 15, 17, 20, 37, 41]. New criteria are used in the comparative study performed in this investigation based on distinguishing between geometry of *actual motion trajectories* (AMT) and track geometry. The AMT curves are described using the motion-dependent Frenet bank, curvature, and vertical development angles, which differ from their counterparts used in the description of the fixed track geometry. Distinction is also made between the *osculating plane*, referred to as the *motion plane*, and the *track plane* [6, 10, 11, 14, 29, 33, 36]. The motion plane is formed by the two vectors tangent and normal to the AMT curves, while the track plane is defined by the value of the track curvature, vertical development, and bank angles. The Frenet bank angle defines the super-elevation of the AMT osculating plane (motion plane), which changes with time as the vehicle moves; while the track super-elevation is motion independent [31, 43]. In this study, particular attention is given to the deviations of the AMT curves from the track centerline curve. It is shown analytically that as the Frenet bank angle increases, the component of the gravity force, which can balance the centrifugal force in its totality, also increases. Computer simulations of the two bogies during curve and tangent track negotiations are performed and the results are presented to compare the three-piece and Y25 bogie performance in specific areas without making a general judgment on the overall bogie performance. Nonetheless, the analysis presented in this investigation, based on the recorded motion trajectories, sheds light on limitations of using *scaled roller rigs* in the prediction of the forces that influence the wheelset and bogie dynamics. The motion trajectories are greatly influenced by the forward motion, and therefore, force interpretation using testing of wheelsets that do not move longitudinally can lead to wrong prediction of the inertia forces as well as the contact forces.

## 2 Performance measures and motion trajectories

The DDS approach used in this investigation to compare the performance of the three-piece and the Y25 bogies is based on recording the motion trajectories using nonlinear MBS computer algorithms, which allow for including model details that are not captured using simplified approaches or linearization techniques. The recorded motion trajectories can be used to accurately determine the centrifugal inertia forces and the time-variant *Frenet bank angle* which differs from the time-invariant track bank angle. The results of the centrifugal force and Frenet bank angle predicted for the two bogies under the same simulation conditions are compared. The details, components, and structures of the three-piece and Y25 bogies will be described in a later Section of this paper.

### 2.1 Recorded motion trajectories

By performing computer simulations, the global position vectors of the bogie components can be recorded to define motion trajectory space curves used to extract the information required to compare the performance of the three-piece and Y25 bogies in specific areas. For a component $i$ of the bogie system, the space curve $\mathbf{r}^i = \begin{bmatrix} x^i & y^i & z^i \end{bmatrix}^T = \mathbf{r}^i(t)$ that defines the global position of the component mass center, the absolute velocity vector $\dot{\mathbf{r}}^i = \dot{\mathbf{r}}^i(t)$, and the absolute acceleration vector $\ddot{\mathbf{r}}^i = \ddot{\mathbf{r}}^i(t)$ can be recorded. The velocity vector can be written as $\dot{\mathbf{r}}^i(t) = \dot{s}\mathbf{r}_s^i$, where $\dot{s} = \left|\dot{\mathbf{r}}^i\right|$ is the magnitude of the velocity along the unit tangent vector $\mathbf{r}_s^i = \partial \mathbf{r}^i / \partial s$, and $s$ is the arc length of the curve $\mathbf{r}^i = \mathbf{r}^i(t)$. The arc length $s$ of the recorded motion trajectory should be distinguished from the arc length used to describe the track centerline and the right and left rail space curves. That is, the velocity vector recorded as function of time can be used to determine the magnitude of the velocity $\dot{s}$ and the unit vector $\mathbf{r}_s^i = \partial \mathbf{r}^i / \partial s$ tangent to the curve. The recorded velocity vector can also be used to determine the partial derivative of the vector $\mathbf{r}^i$ with respect to any of the coordinates $x^i$, $y^i$, and $z^i$ by using the relationship $\dot{\mathbf{r}}^i = \mathbf{r}_\alpha^i \dot{\alpha}^i$, $\alpha^i = x^i, y^i, z^i$, where $\mathbf{r}_\alpha^i = \partial \mathbf{r}^i / \partial \alpha^i$, provided that $\dot{\alpha}^i \neq 0$. For example, if $\dot{y}^i \neq 0$, $\mathbf{r}_y^i = \partial \mathbf{r}^i / \partial y^i = \dot{\mathbf{r}}^i / \dot{y}^i$. The arc length of the motion trajectory curve can also be determined by numerically integrating the differential relationship $ds = \dot{s}dt$.

### 2.2 Centrifugal forces

The recorded motion trajectories can be used to define the centrifugal force vector. To this end, the absolute velocity vector $\dot{\mathbf{r}}^i(t) = \dot{s}\mathbf{r}_s^i$ is differentiated with respect to time to obtain the absolute acceleration vector $\ddot{\mathbf{r}}^i(t) = \ddot{s}\mathbf{r}_s^i + (\dot{s})^2\mathbf{r}_{ss}^i$. This equation can be written as $\ddot{\mathbf{r}}^i(t) = \ddot{s}\mathbf{r}_s^i + \left((\dot{s})^2 / R\right)\mathbf{n}^i$, where $R = 1/\kappa$ is the radius of curvature, $\kappa = \left|\mathbf{r}_{ss}^i\right|$ is the curve curvature, and $\mathbf{n}^i = \mathbf{r}_{ss}^i / \left|\mathbf{r}_{ss}^i\right|$ is the unit vector normal to the motion trajectory curve of the component $i$. Because $\mathbf{r}_s^i$ and $\mathbf{n}^i$ are two orthogonal unit vectors and $\ddot{\mathbf{r}}^i$ is recorded, the dot product of $\mathbf{r}_s^i$ and the acceleration vector $\ddot{\mathbf{r}}^i(t) = \ddot{s}\mathbf{r}_s^i + \left((\dot{s})^2 / R\right)\mathbf{n}^i$ can be used to determine $\ddot{s}$ as $\ddot{s} = \mathbf{r}_s^i \cdot \ddot{\mathbf{r}}^i(t)$. Therefore, the centrifugal inertia force vector is defined as:

$$\mathbf{F}_{ic}^i = m^i\left((\dot{s})^2 / R\right)\mathbf{n}^i = m^i\left(\ddot{\mathbf{r}}^i(t) - \ddot{s}\mathbf{r}_s^i\right) \tag{1}$$

where $m^i$ is the mass of the bogie component. The centrifugal inertia force determined using the recorded motion trajectory will be used to compare the performance of the three-piece and Y25 bogies. As will be discussed, there can be significant centrifugal inertia forces not only during negotiation of a super-elevated curved track, but also during negotiation of a tangent (straight) track because of the nonzero curvature of the motion trajectory curves during the hunting oscillations. Another performance measure that will be used in this study is the Frenet bank angle discussed in the following Section after briefly discussing the MBS approach used to determine the recorded motion trajectories. The Frenet bank angle defines the correct direction of the centrifugal force.

### 2.3 MBS approach

The spatial motion of a rigid body is described using six generalized coordinates, three translational and three rotational. The global position of a point on a body $i$ is defined as $\mathbf{r}^i = \mathbf{R}^i + \mathbf{u}^i = \mathbf{R}^i + \mathbf{A}^i\bar{\mathbf{u}}^i$, where $\mathbf{R}^i$ is the global position vector of the origin of the body coordinate system, $\mathbf{A}^i$ is the transformation matrix that defines the body orientation in the global coordinate system, and $\mathbf{u}^i$ and $\bar{\mathbf{u}}^i$ are the local position vectors of the

point defined in the global and body coordinate systems, respectively [39]. The absolute velocity vectors of the arbitrary point is $\dot{\mathbf{r}}^i = \dot{\mathbf{R}}^i + \boldsymbol{\omega}^i \times \mathbf{u}^i = \dot{\mathbf{R}}^i + \mathbf{A}^i\left(\bar{\boldsymbol{\omega}}^i \times \bar{\mathbf{u}}^i\right)$, where $\boldsymbol{\omega}^i$ and $\bar{\boldsymbol{\omega}}^i$ are the absolute angular velocity vectors defined in the global and the local coordinate systems, respectively. The absolute acceleration vector can be written as $\ddot{\mathbf{r}}^i = \ddot{\mathbf{R}}^i + \left(\boldsymbol{\alpha}^i \times \mathbf{u}^i\right) + \boldsymbol{\omega}^i \times \left(\boldsymbol{\omega}^i \times \mathbf{u}^i\right)$, or $\ddot{\mathbf{r}}^i = \ddot{\mathbf{R}}^i + \mathbf{A}^i\left(\bar{\boldsymbol{\alpha}}^i \times \bar{\mathbf{u}}^i\right) + \mathbf{A}^i\left(\bar{\boldsymbol{\omega}}^i \times \left(\bar{\boldsymbol{\omega}}^i \times \bar{\mathbf{u}}^i\right)\right)$, where $\boldsymbol{\alpha}^i$ and $\bar{\boldsymbol{\alpha}}^i$ are the angular acceleration vectors defined in the global and body coordinate systems, respectively. The velocity and acceleration vectors can be written, respectively, in terms of the four Euler parameters $\boldsymbol{\theta}^i$ as $\dot{\mathbf{r}}^i = \dot{\mathbf{R}}^i - \tilde{\mathbf{u}}^i \mathbf{G}^i \dot{\boldsymbol{\theta}}^i$ and $\ddot{\mathbf{r}}^i = \ddot{\mathbf{R}}^i - \tilde{\mathbf{u}}^i \mathbf{G}^i \ddot{\boldsymbol{\theta}}^i + \boldsymbol{\omega}^i \times (\boldsymbol{\omega}^i \times \mathbf{u}^i)$, where $\tilde{\mathbf{u}}^i$ is the skew symmetric matrix associated with the vector $\mathbf{u}^i$, and $\mathbf{G}^i$ is the matrix that relates the angular velocity vector to the time derivatives of Euler parameters, that is, $\boldsymbol{\omega}^i = \mathbf{G}^i \dot{\boldsymbol{\theta}}^i$. Using this kinematic description, the equation of motion of the system can be written as $\mathbf{M}\ddot{\mathbf{q}} - \mathbf{Q} + \mathbf{C}_\mathbf{q}^T \boldsymbol{\lambda} = \mathbf{0}$, where $\mathbf{M}$ is the system mass matrix, $\mathbf{q}$ and $\mathbf{Q}$ are, respectively, the vectors of system coordinates and generalized forces, $\mathbf{C}_\mathbf{q}$ is the constraint Jacobian matrix, and $\boldsymbol{\lambda}$ is the vector of Lagrange multipliers. The resulting system of differential and algebraic equations (DAEs) is solved numerically to determine the motion trajectories. The algorithm for solving this DAE system is described in detail in the literature [39].

## 3 Frenet bank angle

Track super-elevations are designed to create a lateral gravity force component that balances the lateral component of the centrifugal force. While this lateral force balance is used to define the balance speed, observations of realistic motion scenarios have shown that such force balance is not always achieved leading to significant wheel/rail impact forces which can damage the track structure and lead to accidents. Furthermore, such a force balance is based on the strict assumption that the rail vehicle traces a circular curve that lies in a plane parallel to the horizontal plane, and consequently, the normal to this circular curve and the centrifugal force lie in a plane parallel to the horizontal plane. While this assumption of horizontal centrifugal force is often violated, it is to be noted that, even when using this assumption, the centrifugal force in its totality is not balanced by a component of the gravity force, and such a centrifugal force has a component normal to the track in the direction of the axle load. Because the direction of the centrifugal force is not a priori known, reliance on the current definition of the balance speed without performing extensive computer simulations based on DDS approach to determine the AMT curves will not provide answers that explain the root causes of derailments.

### 3.1 Frenet super-elevation

During the vehicle motion, the centrifugal force in its totality lies in the Frenet osculating plane (motion plane) defined by the vectors tangent and normal to the AMT curves. The *Frenet bank angle* defines the motion-dependent *Frenet super-elevation* of the motion plane. This Frenet super-elevation is unique and differs from the fixed-in-time motion-independent track super-elevation. Furthermore, a nonzero Frenet bank angle and super-elevation may exist when the vehicle negotiates tangent (straight) track segments. Therefore, Frenet super-elevation, which accurately defines the direction of the centrifugal force, allows for better understanding the vehicle dynamics and the force balance during realistic motion scenarios. The uniqueness of the Frenet super-elevation also sheds light on the non-unique definition of the balance speed currently used; the track super-elevation can be increased, and the balance speed can be increased accordingly giving an infinite number of choices.

### 3.2 Frenet–Euler angles

The Frenet bank angle, obtained using a DDS approach, can be used as a measure to compare the performance of the three-piece and Y25 bogies. The Frenet bank angle is a measure of the amount of the Frenet super-elevation that results from the motion of different rail cars or bogies. A larger Frenet bank angle produces a larger component of the gravity force in the motion plane.

It was shown in previous investigations that the unit vectors tangent and normal to the AMT curve can be written in terms of Frenet–Euler angles, referred to for brevity as Frenet angles [31, 42, 43]. These Frenet angles are the *curvature angle* $\psi$, *vertical development angle* $\theta$, and *bank angle* $\phi$. In terms of these angles, the tangent and normal vectors that define the actual motion plane are defined as:

$$\mathbf{r}_s = \dot{\mathbf{r}} \big/ \dot{s} = \begin{bmatrix} x_s \\ y_s \\ z_s \end{bmatrix} = \begin{bmatrix} \cos\psi \cos\theta \\ \sin\psi \cos\theta \\ \sin\theta \end{bmatrix}, \quad \mathbf{n} = \begin{bmatrix} -\sin\psi \cos\phi + \cos\psi \sin\theta \sin\phi \\ \cos\psi \cos\phi + \sin\psi \sin\theta \sin\phi \\ -\cos\theta \sin\phi \end{bmatrix} \tag{2}$$

where $\alpha_s = \partial\alpha/\partial s,\ \alpha = x, y, z$. Because $\mathbf{r}_s = \dot{\mathbf{r}}/\dot{s} = \begin{bmatrix} x_s & y_s & z_s \end{bmatrix}^T$ is known from the recorded trajectory data, as previously discussed, and because the unit normal $\mathbf{n} = \begin{bmatrix} n_1 & n_2 & n_3 \end{bmatrix}^T$ can be determined as the unit vector along the centrifugal force, one can determine the Frenet curvature, vertical development, and bank angles using the definitions of Eq. (2) as

$$\left.\begin{aligned} &\cos\psi = x_s \Big/ \sqrt{(x_s)^2 + (y_s)^2}, \quad \sin\psi = y_s \Big/ \sqrt{(x_s)^2 + (y_s)^2}, \\ &\cos\theta = \sqrt{(x_s)^2 + (y_s)^2}, \quad \sin\theta = z_s, \\ &\cos\phi = (n_2 - y_s n_1) \Big/ \sqrt{(x_s)^2 + (y_s)^2}, \quad \sin\phi = (n_1 + y_s n_2) \Big/ z_s\sqrt{(x_s)^2 + (y_s)^2} \end{aligned}\right\} \tag{3}$$

As discussed in the literature, use of the L'Hopital rule ensures that the Frenet angles in the preceding equation are well defined even in the case of zero curvature [41]. The centrifugal force discussed in the preceding Section and the Frenet bank angle determined in this Section will be used in the DDS approach of this investigation as performance measures.

### 3.3 Gravity force component in the motion plane

It is also clear from the definition of the normal vector in Eq. (2) that the component of the gravity force, in the motion plane which contains the centrifugal force in its totality, is defined as

$$F_{gn} = \begin{bmatrix} 0 & 0 & -mg \end{bmatrix}^T \mathbf{n} = -mgn_3 = mg\cos\theta\sin\phi \tag{4}$$

where $m$ is the vehicle mass and $g$ is the gravity constant. The preceding equation shows that as the Frenet bank angle $\phi$ increases, the component of the gravity force that can balance the centrifugal force also increases.

## 4 Practical considerations in bogie design

The bogie designs have been continuously altered and improved over a long time period that extends more than a century. The goal of the design changes has been to enhance the performance and improve the curving behavior. There are several designs that differ significantly. For example, the two bogies, three-piece and Y25, considered in the numerical study presented in this investigation have different structure, components, joints, and force elements. The Y25 bogie has the frame as the main part, while the three-piece bogie has the bolster and two side frames as its main structural components. In this Section, practical bogie design considerations are discussed to shed light on basic structural differences that will be further discussed when the three-piece and Y25 bogies are described in the following Section.

### 4.1 Background

Developing accurate and efficient computer models for freight trains is challenging because of the large number of friction elements that can be source of problems during the numerical integration of the system equations of motion. In particular, the *friction wedge* used in the three-piece bogie and the *Lenoir link* used in the Y25 bogie are critical elements that require special attention for successful and accurate computer simulations. Developing such accurate computer models of rail vehicles is necessary because of their impact on improving the performance, efficiency, and operating cost [30]. Previous studies have shown that freight cars equipped with three-piece bogies have increased risk of derailment as compared to the Y25 bogie [30, 38]. In this investigation, computer simulations results are used to obtain recorded motion trajectories that allow extracting specific performance measures. Particular attention is given to the deviation of the recorded motion trajectory curve from the track centerline. The centrifugal force is computed using the AMT curve, and new performance measures are considered as previously discussed.

### 4.2 Bogie suspension

The bogie suspension system serves as a vibration isolation that reduces the intensity of the force transmitted to the rail car. Vibrations negatively impact ride comfort in passenger trains and may damage the cargo and

vehicle components of freight trains. Railroad suspensions are often arranged in different directions to absorb not only vertical vibrations but also lateral oscillations due to the wheel/rail contact forces. A suspension system consists of spring and damping elements that can have different arrangements depending on the bogie design. Rubber or air suspension systems, which are more common in passenger trains, are also used as alternatives to coil springs. Friction damping is preferred to conventional hydraulic dashpots because the dissipative damping force is proportional to the weight of the cargo.

Bogie suspension systems can have both *primary* and *secondary suspensions*. Freight cars may have only one of these suspension types: a primary suspension between the wheelsets and bogie frame, referred to as *axle box suspension*; or a secondary suspension between the bogie frame and the car body, referred to as *central suspension* [48]. The primary suspension serves to filter out vertical high-frequency vibrations and contributes to improving lateral stability of the rail vehicle. The secondary suspension serves as isolation of low frequency disturbances and enhances ride comfort. For this reason, secondary suspensions are more common in passenger trains than freight trains. Most passenger trains have both types of suspension to improve the stability and ride comfort.

### 4.3 Primary suspension

The purpose of the primary suspension is to control the transmissibility of the high-frequency wheel/rail contact forces and reduce derailment risk, vibrations, and noise [44]. *Leaf springs*, also known as *horns*, which rest on the axle box and their ends are connected to the frame by double links attached to pins located on the underframe, were more common in the past [46]. The leaf-spring suspension provides also damping as the result of friction between the spring leaves. This kind of suspension is still popular in Europe, particularly for new two-axle freight wagon applications. However, leaf-spring suspensions are becoming less common in modern trains because of possible defects, particularly during braking that can lead to cracks. Furthermore, the spring elasticity can deteriorate when the spring is subjected to high pressures that cause wear of the friction surfaces [48]. For these reasons, leaf springs are replaced by coil springs which can have different arrangements including use of two cylindrical stubs wrapped by coil springs. A collar mounted on the axle box can slide vertically on the stubs under the effect of the springs. An alternative is the rubber shear block, made of rubber enforced by steel leaves [48]. While leaf-spring problems resulting from braking are avoided when using coil springs, damping elements such as hydraulic or friction elements are needed for the energy dissipation.

### 4.4 Secondary suspension

The secondary suspension, which connects the car body to the bogie frame, normally consists of a combination of air springs and rubber or metal bearers that restrict vertical, lateral, and torsional displacements [44]. A secondary suspension system is used in most passenger trains and in some freight trains. While in the past coil springs were more common for the secondary suspension, air springs are now preferred because of their variable stiffness which makes them more effective in covering a wider range of frequencies and loads. Despite their complexity and higher cost, air springs are lighter and provide better sound isolation, and their stiffness can be tuned electronically.

Freight trains may have only primary suspensions because the ride comfort is not a priority despite the fact that it is always recommended to reduce or control the vibration level. In freight trains without secondary suspensions, the car body is directly mounted on a steel plate which is supported by the primary suspension. A central pin connects the car body to the plate center to provide the rotational degree of freedom needed for safe curve negotiations. Two side bearers are placed to the right and the left of the pin to provide a stable support for the car body, which can slide on these plates while rotating [12].

### 4.5 Single wheelset versus bogies

The single-wheelset running gear is mainly used for rail cars supported by two axles only. In this configuration, the rail car is mounted on two wheelsets, one in the front and one in the back. Leaf springs mounted on the axle box and connected to the car frame by two swing hangers can be used as the primary suspension, called *double-link suspension*. The axle box bearings allow the wheelset axles to rotate independently from the other components of the vehicle, while the leaf springs allow longitudinal and lateral oscillations of the axle box with respect to the car frame. The longitudinal suspension stiffness is higher than the lateral stiffness because of the leaf orientation. The leaf-spring damping mechanism has advantage of being load-sensitive at the expense of

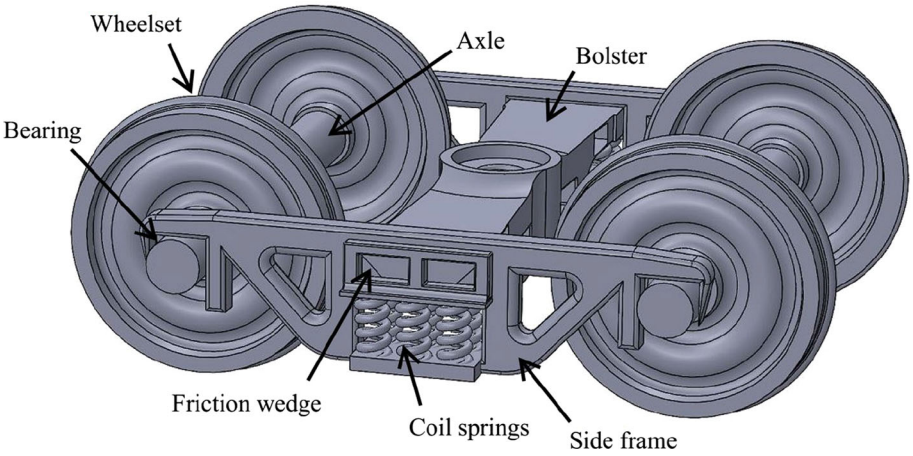


**Fig. 1** Three-piece bogie

exposure of the spring leaves, that generate the friction, to the atmosphere, dirt, and humidity that influence the spring effectiveness [21]. The single-wheelset running gear has been used in the past because of its simplicity, low cost, robustness, and limited space required. However, two-axle freight cars with double-link suspension have poor hunting characteristics because of low level of lateral damping. Moreover, due to corrosion and wear, suspension parameters can change significantly during the vehicle life [22]. For this reason, despite that single-wheelset cars are still used in Europe, current trend in industry is to use freight bogies.

While a bogie mainly consists of wheelsets, bearings, and a suspension system, it can also include a steering mechanism, brake system, lubrication devices, monitoring sensors, and other subsystems. Most modern trains are equipped with bogies containing two axles, and each rail car is usually mounted on two bogies, one on the front and one on the back. Another alternative is to connect two cars using the *Jacobs design*, in which each bogie supports the ends of two consecutive cars. This configuration increases the axle load but improves the ride performance and reduces the vehicle masses [44]. One of the first popular bogie models was the link suspension bogie, also known as *G bogie*, standardized in Europe by the International Union of Railways (UIC) in the 1950s [24]. This bogie design has four double-link suspensions with leaf springs connecting two wheelsets to a bogie frame on which the rail car is mounted. The evolution of the suspension systems in the second half of the twentieth century led to more sophisticated bogie models which are commonly used in modern trains. Two of most commonly used freight bogies are the *three-piece* and *Y25 bogies*, discussed in the following Section and considered in this study.

## 5 Three-piece and Y25 bogies

In this Section, the three-piece and the Y25 bogies used in this investigation are discussed. The results obtained using the DDS computational approach are used in this investigation to extract performance measures that shed light on the bogie behavior and the effectiveness of the gravity force in balancing the centrifugal force.

### 5.1 Three-piece bogie

The three-piece bogie design, shown in Fig. 1, was developed in the USA and is widely used in many other countries. The bogie design has been continuously changed and improved over many decades, leading to different design configurations adopted by different countries, including countries in North and South Americas, Russia, China, India, Australia, and African countries. Use of the three-piece bogies is common for heavy vehicles because of their high permissible axle load that reaches 36 tons [22]. While these bogies are very durable, their structure is simple and compact, they require low production and maintenance cost, and their repair and maintenance is simple. However, three-piece bogies have some disadvantages that include higher risk of derailment during curve negotiations and dynamic instability when used with unloaded cars. They also exert higher dynamic loads on the track because of lack of a double suspension system, and this in turn causes increased wear of the wheel and rail surfaces, resulting in higher vibration level and track-maintenance cost [38].

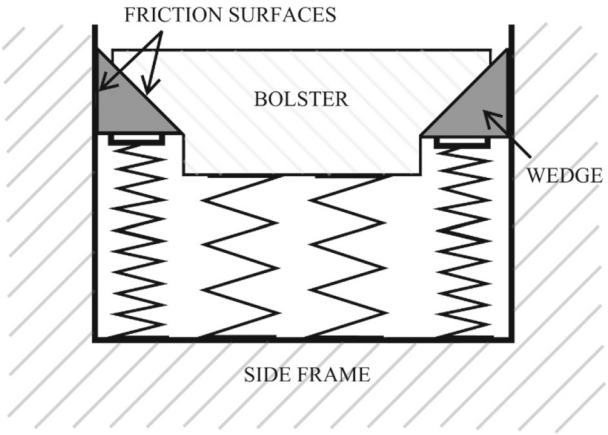


**Fig. 2** Friction wedge mechanism

The three-piece bogie, as its name indicates, consists of three main parts: bolster and two side frames. The two wheelsets of the bogie are connected to the two side frames by four sets of bearings located at the right and left ends of the axles. The side frames are longitudinal rigid structures on which the bolster is installed horizontally using a suspension system that consists of two sets of coil springs and four friction wedges divided between the two side frames. The coil springs serve to isolate the vibration, and the friction wedges serve as energy-dissipating elements that are alternatives to the hydraulic or pneumatic dampers used in passenger trains. Friction wedges are more common for freight trains because they produce higher friction forces as the axle load increases. A friction wedge, which is a triangular steel block vertically supported by a spring, can be arranged in two different configurations: *constant damping* and *variable damping*. In the constant damping configuration, the spring supporting the wedge is attached to the bolster; while in the variable damping configuration, the spring is attached to the lower part of the side frame [45]. The variable damping arrangement, shown in Fig. 2, is more common, and it is the configuration used in this study. In this configuration, each wedge has a face in contact with a vertical surface of the side frame, while the inclined surface of the wedge is in contact with the bolster. During operation, the friction force resulting from the relative sliding between the contact surfaces leads to energy dissipation proportional to the axle load. The car body is mounted on the *center plate*, centrally placed on the bolster, using a revolute joint that allows for a relative rotation required for improved performance during curve negotiations.

### 5.2 Y25 bogie

The Y25 bogie, shown in Fig. 3, is the second most widely used bogie in modern freight trains. It was developed in France in 1948, and it was standardized in 1967 by the ORE (Office de Recherches et d'Essais) committee [22]. The main components of this bogie are two wheelsets, four axle boxes, four spring holders, and a frame. As in the three-piece bogie, sets of bearings, placed in axle boxes, are used at the ends of the wheelset axles. The frame is a single rigid structure extended along the whole bogie, and it is supported by the primary suspension that consists of four sets of vertical coil springs mounted on the axle boxes. Unlike the three-piece bogie, the suspension is placed closer to the wheels. The damping in the vertical direction is generated by a mechanism called *Lenoir link*, designed to use part of the cargo weight to generate friction that is load-sensitive and proportional to the weight of the car body [24]. A Lenoir link, shown in Fig. 4, connects the frame to a spring holder, which is a cap-like device fixed to the tip of one of the springs vertically mounted on the axle box. The spring which supports the spring holder is always the most internal component in the axle box with respect to the center of the bogie, as shown in Fig. 3. The Lenoir link is inclined to allow converting the car weight to horizontal and vertical components at the spring holder [3]. The vertical component is absorbed by the spring deformation, while the horizontal component is transmitted by the holder to a pusher that is pressed against a vertical surface on the axle box. The vertically oscillating spring holder drags the pusher up and down, generating friction force proportional to the normal force applied by the pusher. This friction mechanism is comparable to the one provided by the friction wedges of the three-piece bogie. The Y25 bogies can also have a secondary suspension consisting of two sets of coil springs located between the frame and

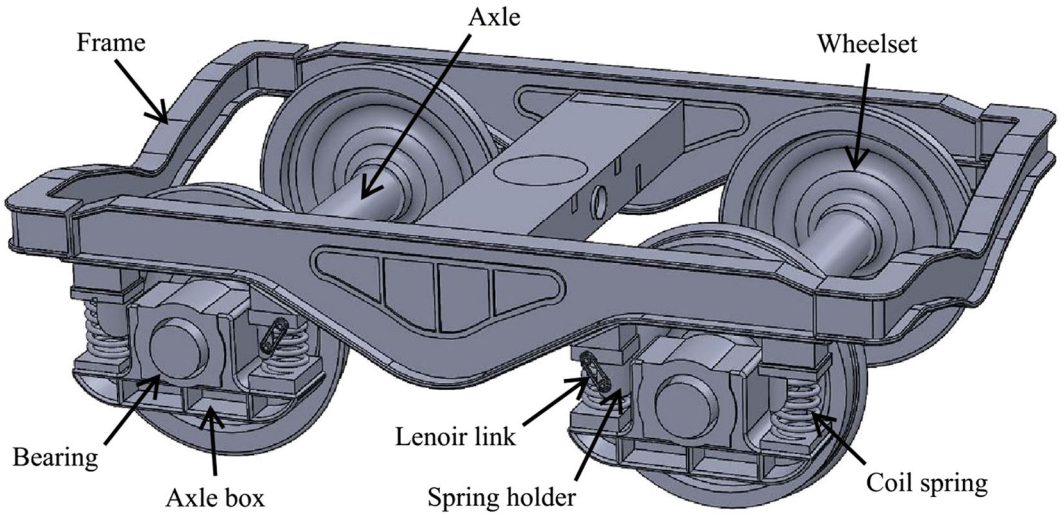


**Fig. 3** Y25 bogie

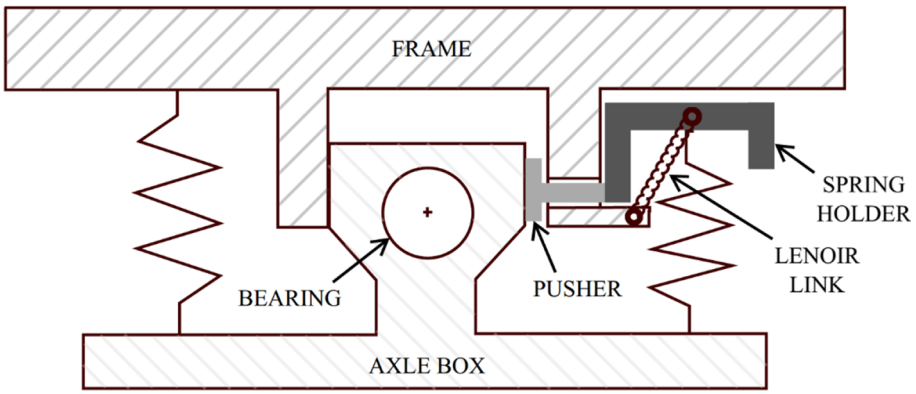


**Fig. 4** Lenoir link mechanism

the car body. While the admissible Y25 axle loads are not as high as allowed by three-piece bogies, previous studies reported lower risk of derailment during curve negotiations for the Y25 bogie [30].

## 6 Geometry considerations and balance speed

It was shown that the component of the gravity force that balances the centrifugal force in its totality is given in terms of the Frenet vertical development and bank angles $\theta$ and $\phi$, respectively, by $F_{gn} = mg\cos\theta\sin\phi$. This equation demonstrates that for zero Frenet bank angle $\phi$, there is no gravity force component that lies in the motion (osculating) plane regardless of whether or not there is a centrifugal force. The centrifugal force exists when a vehicle traces a curve which may or may not have zero Frenet bank angle. For example, a mass that traces a *helix curve* has a centrifugal force while the Frenet bank angle $\phi$ of the helix curve is zero [31, 43]. In this case, there is no gravity force component that can be used to balance the centrifugal force. For this reason, the concept of the *Frenet super-elevation* is fundamental for understanding the forces that influence the vehicle motion. The Frenet super-elevation should be distinguished from the track super-elevation, which has proven to be less effective and does not totally prevent wheel/rail flange contacts, despite its contribution to lower the severity of the impacts.

### 6.1 Track super-elevation

The track super-elevation is used in practice for curved track segments to create a lateral component of the gravity force that balances the lateral component of the centrifugal force. The curved segments of the track

are super-elevated by a track bank angle $\phi_t$ which is different from the Frenet bank angle $\phi$. An assumption is made that the vehicle strictly traces a circular curve that lies in a plane parallel to the horizontal plane, and consequently, the centrifugal force in its totality, $m(V)^2/R_t$, is assumed to lie in this plane, where $V$ is the forward velocity of the vehicle along the tangent to the circular curve, and $R_t$ is the radius of curvature of the circular curve. In this case, the lateral component of the centrifugal force is $\left(m(V)^2/R_t\right)\cos\phi_t$ and the lateral component of the gravity force is $mg\sin\phi_t$. By equating these two force components, the balance speed is defined as $V = \sqrt{gR_t\tan\phi_t} = \sqrt{gR_th/G}$, where $h$ and $G$ are, respectively, the track super-elevation and gage. This definition of the balance speed lacks uniqueness, because the bank angle $\phi_t$ can be increased and the balance speed $V$ can be increased accordingly. Furthermore, observations of realistic motion scenarios have shown that use of this definition of the balance speed does not prevent wheelsets from moving toward the high and low rails, exerting high impact forces on the rail structure, and maintaining undesirable continuous wheel/rail contact during curving. Therefore, extensive computer simulations performed to obtain recorded motion trajectories offer alternatives for extracting information that will eventually lead to more proper force interpretation.

### 6.2 Forward motion and roller test rigs

The forward velocity $V$ along the tangent to the track center line, needs to be distinguished from the velocity $\dot{s}$ along the tangent to the motion trajectory curve. An approximate relationship between the two velocities can be obtained from the definition of the motion trajectory curve velocity vector $\dot{\mathbf{r}}^i = \left[\dot{x}^i \;\; \dot{y}^i \;\; \dot{z}^i\right]^T$ of component $i$. If the trajectory coordinates are used, one can write [40]

$$\begin{aligned}\dot{\mathbf{r}}^i &= \left[\dot{x}^i \;\; \dot{y}^i \;\; \dot{z}^i\right]^T = \left[\dot{s}_t^i \;\; \dot{y}_t^i \;\; \dot{z}_t^i\right]^T \\ &= \mathbf{r}_s^i\dot{s}^i = \dot{s}^i\left[r_{s1}^i \;\; r_{s2}^i \;\; r_{s3}^i\right]^T\end{aligned} \tag{5}$$

where $s_t^i$ is the arc length of the track centerline, and $y_t^i$ and $z_t^i$ are, respectively, the displacements in the lateral and normal directions with respect to the track centerline. The preceding equation shows that $\dot{s}_t^i = \dot{s}^i r_{s1}^i$. This equation and the definition of the inertia force vector $\mathbf{F}_i^i = m^i\ddot{\mathbf{r}}^i(t) = m^i\left(\ddot{s}\mathbf{r}_s^i + \left((\dot{s})^2/R\right)\mathbf{n}^i\right)$ shed light on the limitation of roller test rigs in which the wheelset forward motion is replaced by rotating rollers that represent the rails. Given the influence of the inertia forces on the dynamics and forces of wheelsets and the wheel/rail contact, the serious limitations of using roller test rigs are obvious. The forward motion has a significant effect on the geometry of the motion trajectory curves and on the definitions of the unit tangent and normal vectors $\mathbf{r}_s^i$ and $\mathbf{n}^i$, respectively.

### 6.3 Frenet force balance and recorded motion trajectories

Recorded motion trajectories can be accurately measured using vehicles instrumented with advanced sensors, or can be obtained using computer simulations of detailed virtual models. To have proper force interpretation, it is important to distinguish between the geometry of the track and the geometry of the motion trajectory. This distinction can be made by distinguishing between the track curvature, vertical development, and bank angles denoted, respectively, as $\psi_t, \theta_t$, and $\phi_t$; and the motion trajectory Frenet curvature, vertical development, and bank angles $\psi, \theta$, and $\phi$, respectively. For example, on a tangent track, the track curvature, vertical-development, and bank angles can all be zero, that is, $\psi_t = 0$, $\theta_t = 0$, and $\phi_t = 0$; while the Frenet angles are different from zeros because of the hunting oscillations which define motion trajectory curves with Frenet curvature, vertical development, and bank angles that can be different from zero.

The recorded motion trajectory curves can be used to provide precise definition of the *balance speed*; this is with the understanding that motion trajectories are not a priori known. Nonetheless, a more precise definition of the balance speed based on extensive computer simulations can create the knowledge and provide force interpretations that allow for developing more credible operation and safety guidelines. The definition of the balance speed based on the fixed track geometry and given by $V = \sqrt{gR_t\tan\phi_t} = \sqrt{gR_th/G}$ is derived using a strict assumption that cannot be fulfilled in realistic motion scenarios and does not account for the actual motion and forces acting on the system. To develop a more precise definition based on the assumption that $V = \dot{s}_t^i = \dot{s}^i r_{s1}^i$ is the operating vehicle velocity, an osculating-plane force balance can be used. It is clear from the equation $V = \dot{s}^i r_{s1}^i$ that in the case of a forward motion with non-zero $V$, $\dot{s}^i r_{s1}^i \neq 0$. The osculating-plane component of the gravity force is $F_{gn} = mg\cos\theta\sin\phi$, and the centrifugal force, which is in the direction of

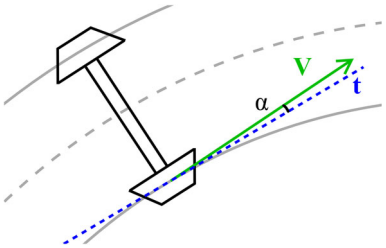


**Fig. 5** Angle of attack

the normal vector that lies in the osculating plane, is defined as $m\left(\dot{s}^i\right)^2/R = m\left(V/r_{s1}^i\right)^2/R$. Equating these two osculating-plane force components, a precise definition of the balance speed can be obtained as

$$V = r_{s1}^i\sqrt{Rg\cos\theta\sin\phi} \tag{6}$$

Because $R$ is the radius of curvature, the definition of the balance speed given by the preceding equation is function of all the three Frenet angles which are motion dependent. The only constant in this definition is the gravity constant $g$. It is also important to point out a fundamental difference between the balance speed in the preceding equation and the balance speed definition based on the motion-independent track geometry. The definition of the balance speed in the preceding equation assumes that the osculating-plane component of the gravity force balances the centrifugal force in its totality. In the definition used in practice, on the other hand, the lateral component of the gravity force is assumed to balance only the lateral component of the centrifugal force.

### 6.4 Angle of attack

Another geometric measure for the bogie curving behavior is the *angle of attack* of a wheelset, defined as the angle between the forward velocity vector of the wheelset and the longitudinal tangent to the rail at the contact point. That is, the angle of attack $\alpha$ is defined as $\alpha = \cos^{-1}\left(\mathbf{V}^w \cdot \mathbf{t}^r \big/ |\mathbf{V}^w||\mathbf{t}^r|\right)$, where $\mathbf{V}^w$ is the wheel velocity vector and $\mathbf{t}^r$ is the longitudinal rail tangent at the wheel/rail contact point. The angle of attack defines orientation of the wheelset with respect to the rail as shown in Fig. 5. A smaller angle of attack is an indication that the wheelset is following the track curve; while a larger angle of attack indicates a larger deviation from the desired trajectory and the possibility of wheel climb. Previous investigations have shown that the angle of attack is related to and influenced by the wheel/rail contact forces and slippage and has an effect on the wear of the rail and wheel flange surfaces [19]. The value of the angle of attack is related to the distance required for a complete wheel climb; the larger the angle of attack is, the higher the risk of derailment due to wheel climb [25]. Previous studies have shown that the angle of attack of a wheelset travelling on a track with variable radius of curvature generally ranges from 0 to 0.5° [7, 19, 25].

## 7 Concept demonstration

In this Section, a simple example is used to demonstrate the concepts discussed in this investigation before presenting the three-piece- and Y25- bogie results in the following Section. For this purpose, a single unsuspended wheelset model travelling freely on a curved track with a forward velocity 15 m/s is used. The wheelset is subjected to an initial lateral velocity of 0.3 m/s to initiate the hunting oscillations. The track used in this example is the same as the one described in Sect. 8.3. The wheelset mass is assumed 1568 kg, and the mass moments of inertia are $I_{xx} = I_{zz} = 656$ kg.m$^2$ and $I_{yy} = 168$ kg.m$^2$. The wheelset is considered rigid and equipped with the APTA 120 wheels described in more detail in Sect. 8.4.

Figure 6 shows the track bank angle $\phi_t$ for various track sections that include tangent, spiral, and curve sections. The results presented in this Figure show that the track bank angle is zero for the tangent sections and nonzero for the spiral and curve sections. The magnitude of the wheelset centrifugal force is shown in Fig. 7 for two cases. The first is the magnitude of the centrifugal force computed using the track geometry and defined as $m(V)^2\big/R_t$, while the second is the magnitude of the centrifugal force obtained using the recorded motion trajectories and is defined as $m(\dot{s})^2\big/R$. Superscript $i$ is removed for simplicity of the figure-caption notation. It is clear from the results presented in Fig. 7 that there is a significant difference between the magnitudes of

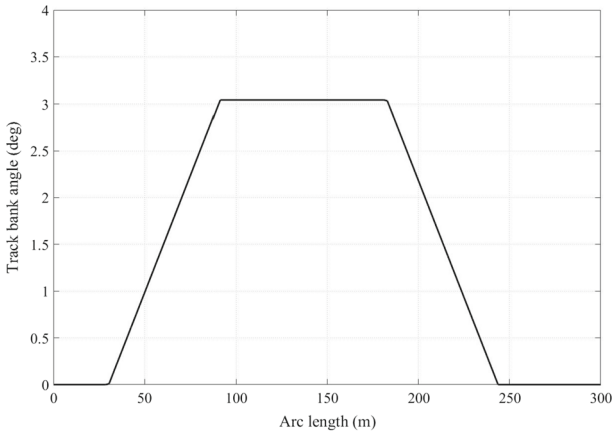


**Fig. 6** Track bank angle

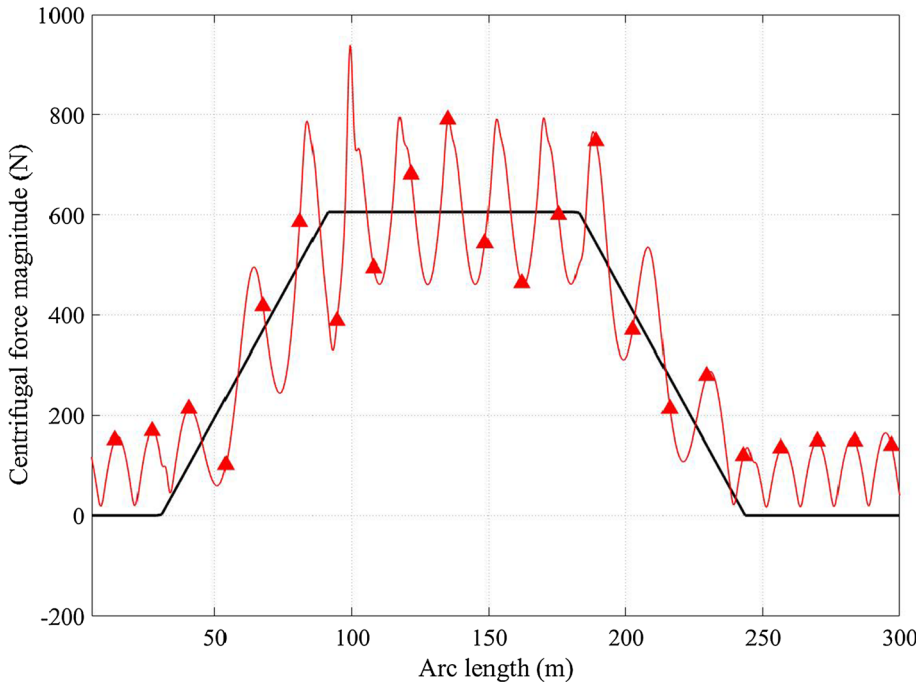


**Fig. 7** Centrifugal force for the unsuspended wheelset (—$m(V)^2/R_t$, —▲—$m(\dot{s})^2/R$)

the two forces, and such a difference cannot be ignored even in the case of a simple wheelset with a mass much smaller than the laden freight cars. Furthermore, the magnitude of the centrifugal force computed using the motion trajectories is oscillatory reflecting the nature of the hunting oscillation of the wheelset. These oscillations are not captured by the definition of the centrifugal force used in practice based on the motion-independent track geometry. Furthermore, as previously discussed, the centrifugal force can be significantly different from zero when negotiating the tangent sections of the track as demonstrated by the results presented in Fig. 7. To verify the tangent section results presented in Fig. 7, the centrifugal force along the tangent segments is computed using the equation $|\mathbf{F}_{\text{ice}}| = m(\omega_h)^2 Y_h \sin(\omega_h t + \beta)$, derived from Klingel's geometrical analysis, where $m$ is the wheelset mass, $t$ is time, $\omega_h$ and $Y_h$ are, respectively, the frequency and amplitude of the hunting oscillations, and $\beta$ is a phase angle [40, 42]. The tangent track centrifugal force results obtained using this simple equation based on pure geometric analysis show a remarkable agreement with the results obtained using the fully nonlinear MBS simulation of the wheelset. The results of the track bank angle shown in Fig. 6 are consistent with the prediction of the centrifugal force as defined by the track geometry.

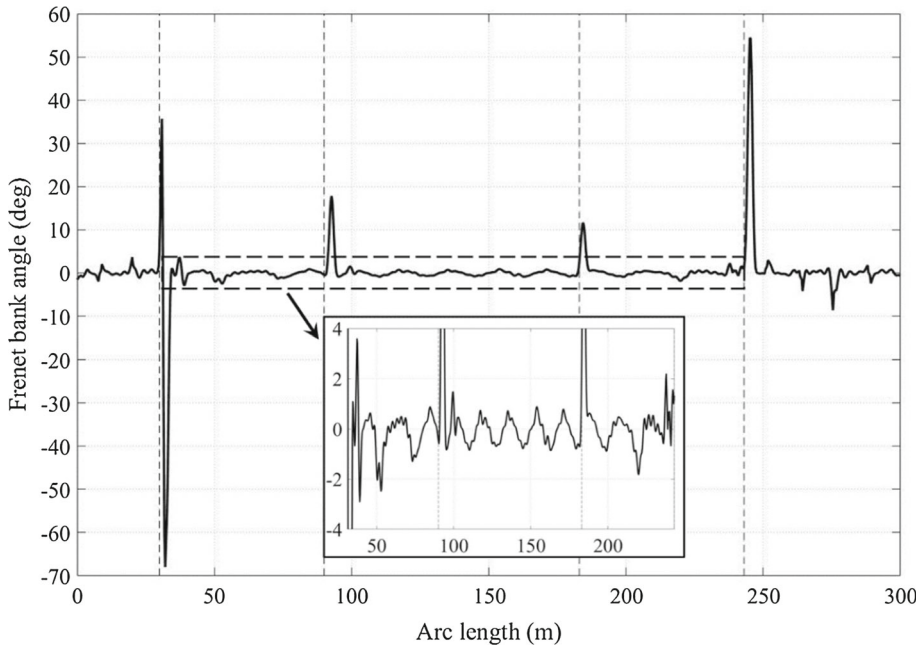


**Fig. 8** Unsuspended wheelset Frenet bank angle

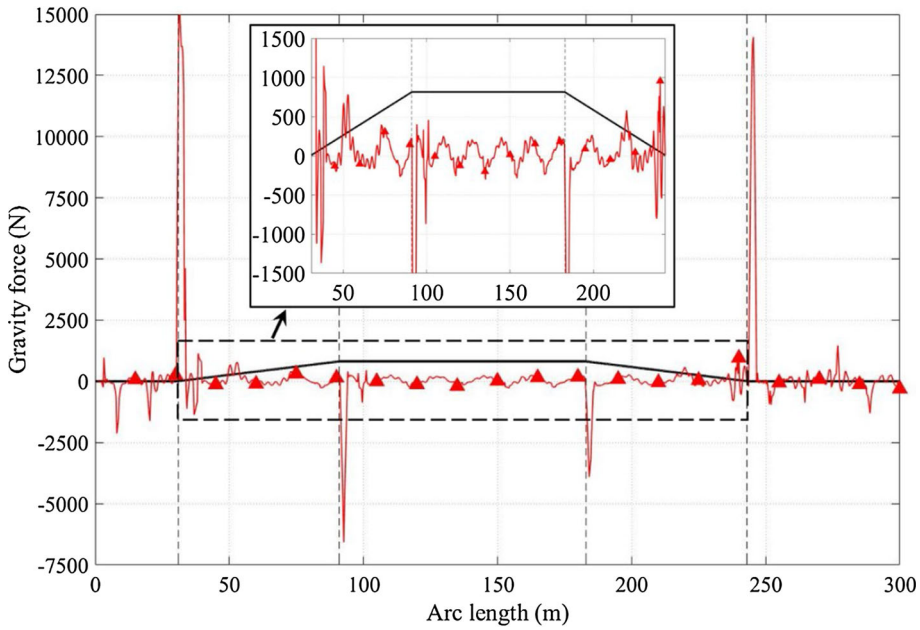


**Fig. 9** Gravity force component in the track and osculating plane (— Track plane, —▲— Osculating plane)

To analyze the direction of the centrifugal force vector, which is parallel to the unit vector normal to the curve, the Frenet bank angle obtained using the motion trajectory curve is plotted in Fig. 8 and compared with the track bank angle. Zoomed plots are used to demonstrate the differences since bank angles are normally small and their amplitude can be small in comparison with the values due to the discontinuities at the track transitions. The results of the track and Frenet bank angles presented in Fig. 8 show differences attributed to the fundamental difference in the definition of these two angles; one is motion-independent, while the other is motion dependent. Furthermore, the Frenet bank angle is sensitive to the discontinuities at the track-section transitions at which higher degrees of continuity are not enforced. The track bank angle obtained by linear interpolation does not exhibit this sensitivity. An important and interesting observation from the results shown in Fig. 8 is the large Frenet bank angle when the wheelset negotiates the tangent sections of the track due

to the hunting oscillations. By examining the zoomed plot, it is possible to see that the Frenet bank angle varies between -1° and 1° and it has oscillations similar to the centrifugal force oscillations. Figure 9 shows a comparison between components of the gravity force in the track plane and osculating plane. The former is defined by the equation $mg \sin \phi_t$, while the latter is defined by the equation $mgn_3$, where $n_3$ is the third element of the unit vector normal to the motion trajectory curve.

## 8 Bogie/track simulation models

In this Section, computer simulation models of the three-piece, Y25 bogies, track, and friction contact are described. The computer models are analyzed using a nonlinear MBS algorithm based on a three-dimensional wheel/rail contact formulation. Each bogie model consists of several rigid bodies interconnected by joints and force elements. The bogie models are assumed to travel on a track with tangent, spiral, and curve sections. Because the inertia, material, and geometric properties used in this investigation are not exact, the kinematic and force results will be presented in the following section without making judgments on the overall bogie performance, as previously mentioned. Therefore, the results presented in the following Section serve to explain new concepts used in the *Frenet force balance*. The motion trajectories will be obtained using the software SIGMA/SAMS (Systematic Integration of Geometric Modeling and Analysis for the Simulation of Articulated Mechanical Systems).

### 8.1 Three-piece bogie model

The three-piece bogie model used in this Section is based on the model presented by Sun and Cole [45]. This bogie model, despite its simplicity, can exhibit simulation instabilities due to the nonlinear characteristics of its friction elements. The bogie model is assumed to consist of nine bodies: two wheelsets, two side frames, four friction wedges, and a bolster. The distance between front and rear wheelsets is 2.591 m, and the bolster center of mass has initial vertical position of 0.457 m. The inertia properties used in the simulations are listed in Table 1.

The leading wheelset of the bogie is assumed to travel with a prescribed constant forward velocity of 17.4 m/s along the track centerline. The side frames are attached to the ends of the wheelsets axles by bearing elements which generate forces proportional to the relative displacement and velocity between the two bodies connected by the bearing elements. The bearing stiffness and damping coefficients are assumed $1.75 \times 10^7$ N/m and $1.75 \times 10^5$ N.s/m, respectively. Side frames are connected to the bolster by springs modeled using bushing elements. In the computer model, two vertical-axis springs are used to connect each side frame to the bolster. The springs have a vertical stiffness coefficient $1.69 \times 10^6$ N/m, vertical preload $4 \times 10^4$ N, and lateral and longitudinal stiffness coefficients $1 \times 10^6$ N/m. In this arrangement, the lateral and longitudinal stiffness is approximately 60% of the stiffness in the vertical direction. The same vertical stiffness and preload are used for the springs that support the friction wedges, each is assumed to have mass of 10 kg. The bolster, placed transversally with respect to the side frames, is modeled as a rigid beam whose ends are located just above the wedges. Each wedge has a vertical friction surface in contact with the side frame and 45° inclined friction surface in contact with the bolster. The friction surface formulation is explained in more detail in Sect. 8.5. The bolster has the freedom to move vertically with respect to the side frames, but the relative yaw rotation and longitudinal displacement are restricted by using two vertical-axis cylindrical joints between the side frames and the ends of the bolster.

### 8.2 Y25 bogie model

The Y25 bogie model used in this study is based on the model proposed by Bosso et al. [3]. The bogie components considered are two wheelsets, four axle boxes, four spring holders, and a frame. The distance

**Table 1** Inertia parameters for the three-piece bogie model

| Wheelsets | Side frames | Bolster | Friction wedges |
|---|---|---|---|
| $m = 1500$ kg | $m = 469$ kg | $m = 500$ kg | $m = 10$ kg |
| $I_{xx} = 420$ kg·m$^2$ | $I_{xx} = 100$ kg·m$^2$ | $I_{xx} = 175$ kg·m$^2$ | $I_{xx} = 0$ kg·m$^2$ |
| $I_{yy} = 120$ kg·m$^2$ | $I_{yy} = 115$ kg·m$^2$ | $I_{yy} = 10$ kg·m$^2$ | $I_{yy} = 0$ kg·m$^2$ |
| $I_{zz} = 420$ kg·m$^2$ | $I_{zz} = 115$ kg·m$^2$ | $I_{zz} = 175$ kg·m$^2$ | $I_{zz} = 0$ kg·m$^2$ |

**Table 2** Inertia parameters for the Y25 bogie model

| Wheelsets | Axle boxes | Spring holders | Frame |
|---|---|---|---|
| $m = 1225$ kg | $m = 50$ kg | $m = 5$ kg | $m = 5500$ kg |
| $I_{xx} = 750$ kg·m$^2$ | $I_{xx} = 0$ kg·m$^2$ | $I_{xx} = 0$ kg·m$^2$ | $I_{xx} = 1400$ kg·m$^2$ |
| $I_{yy} = 140$ kg·m$^2$ | $I_{yy} = 0$ kg·m$^2$ | $I_{yy} = 0$ kg·m$^2$ | $I_{yy} = 2000$ kg·m$^2$ |
| $I_{zz} = 750$ kg·m$^2$ | $I_{zz} = 0$ kg·m$^2$ | $I_{zz} = 0$ kg·m$^2$ | $I_{zz} = 2500$ kg·m$^2$ |

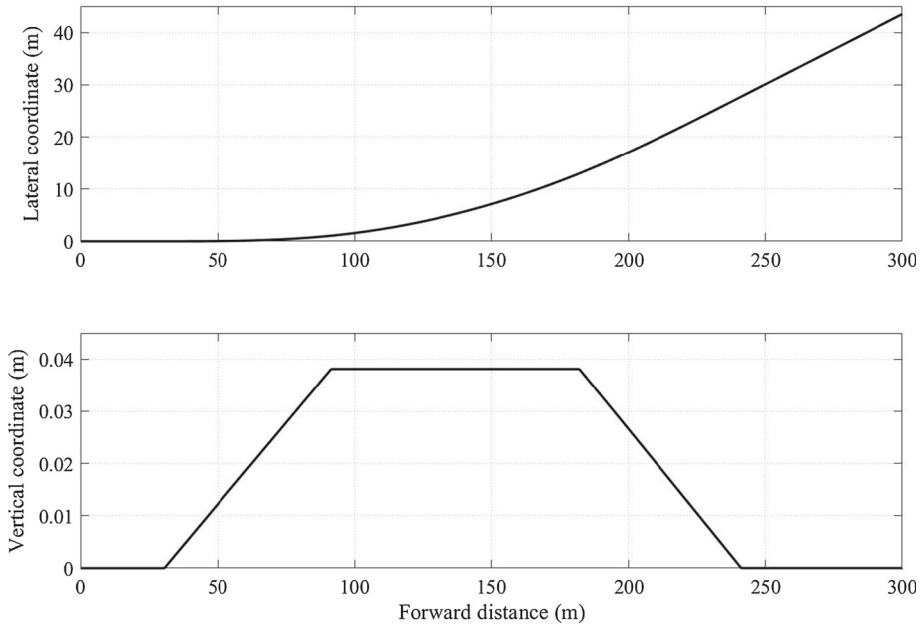


**Fig. 10** Track geometry

between the front and rear wheelsets is assumed 2.591 m, and the center of mass of the frame has the same initial vertical position of 0.457 m. The inertia properties used in the computer simulations are provided in Table 2. The front wheelset has a prescribed forward velocity 17.4 m/s. The axle boxes are connected to the ends of the wheelset axles using bearing elements. For the first suspension, two vertical springs are attached to each wheelset: one supports the frame and the other supports a spring holder. These springs are modeled using bushing elements with the same parameters as those used for the three-piece bogie model. The Lenoir links connecting the four spring holders to the frame are modeled as bushing elements, but with a relatively high stiffness, equal to $2 \times 10^7$ N/m, to ensure negligible link deformation and direct force transmission from the frame to the spring holder. Because Lenoir links are inclined 60° with respect to the horizontal plane, the transmitted force has vertical and horizontal components. The friction is considered using vertical friction contact surfaces between each spring holder and an axle box. During the motion, the bushing element, representing the Lenoir link, pushes the spring holder against the axle box, and friction forces are generated.

### 8.3 Track model

The 300-m track model used has 1.435 m gage and starts with 30 m tangent segment, followed by 60 m spiral for transition to a left 90–m-3-degree curve with radius of curvature 582 m, followed by a 60 m spiral segment to connect with 60 m tangent segment. Considering a constant vehicle speed of 17.4 m/s, the total travel time is approximately 18 s. Figure 10 shows the track geometry defined by its lateral and vertical coordinates.

The rail profile used in the three-piece bogie simulation is the standard 140-lb wheel profile given by AREMA (American Railway Engineering and Maintenance-of-Way Association). For the Y25 bogie simulation, a standard UIC54 rail, manufactured according to European Standard EN 13,674–1, is adopted.

In developing the track model, a preprocessor computer program is used to determine a track point-mesh geometry data file based on the standard industry inputs: horizontal curvature, grade, and super-elevation. These standard industry inputs at points at which the track geometry changes are used to define position coordinates

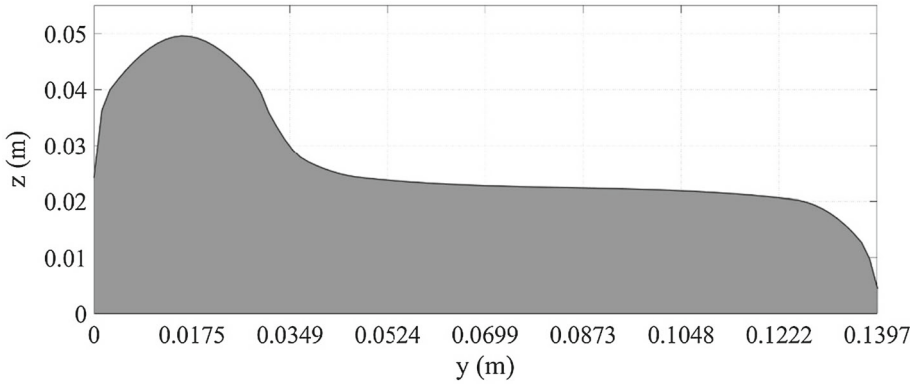


**Fig. 11** APTA 120 wheel profile

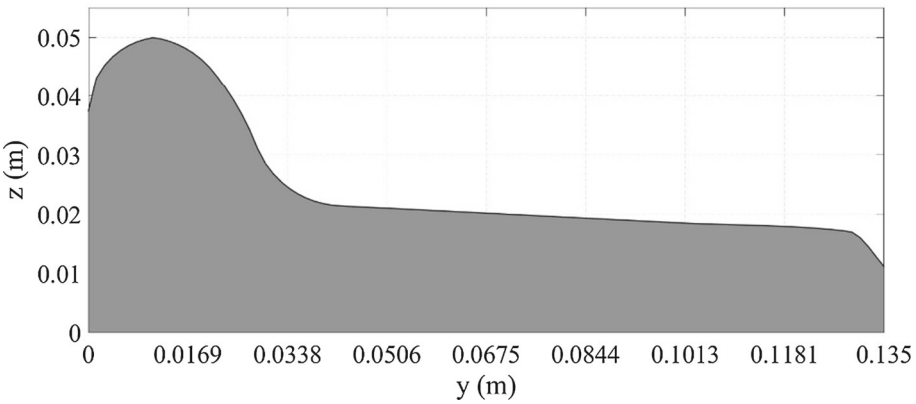


**Fig. 12** P1 wheel profile

and orientation angles at nodal points. The position and angle coordinates are used with an interpolation based on the *absolute nodal coordinate formulation* (ANCF) to define the track geometry at arbitrary points within the segments defined by the track nodes. This ANCF representation ensures gradient continuity at the nodes but does not ensure curvature continuity at the track transitions. Because of this numerical representation, spikes can be observed in the numerical results due to the curvature discontinuities at the intersections of track segments with different curvature values.

### 8.4 Wheel profiles

The wheelsets have axles with diameter 0.1 m and length of 2.06 m. Freight trains standard wheel diameters range from 840 to 920 mm, while the standard width is approximately 130 mm [46]. The wheel diameter and width used in the simulations are, respectively, 914 mm and 135 mm. Two different wheel profiles are used for the two bogies: an American standard for the three-piece bogie and a European one for the Y25 bogie. For the three-piece bogie, the APTA 120 profile is chosen. This profile, provided by the American Public Transportation Association (APTA), is based on an older AAR S-621-79 profile previously proposed by the Association of American Railroads (AAR). The APTA 120 profile has conicity of 1:20 (5% slope), flange angle 72°, and flange height 1 inch [47]. For the Y25 bogie, the P1 profile extracted from the Railway Group Standard GMRT2466 is chosen. This profile, based on BR (British Rail) drawing S8 C2-8,006,234, has tread slope of 5%, flange angle 60°, and flange height 29.93 mm [34]. The two wheel profiles are shown in Figs. 11 and 12. The friction coefficient between the wheels and rails is assumed 0.5, and the wheel and rail materials are assumed steel with modulus of elasticity 210 GPa and shear modulus 82 GPa.

### 8.5 Friction elements

Friction damping forces are challenging to model and can be source of numerical instability. In the three-piece bogie, there are eight friction contacts: four on the inclined surfaces between the bolster and wedges, and the

other four on the vertical surfaces between wedges and side frames. In the case of the Y25 bogie, on the other hand, there are four friction contacts between the spring holders and axle boxes. A compliant force model is used in this study to model all friction contacts. In this compliant force model, the force component normal to the contact surfaces is assumed to have an elastic-force term proportional to the surface penetration $\delta$ and damping force term proportional to the penetration rate. The penetration between two bogie components $i$ and $j$, projected along the direction of the outward normal to the contact surfaces $\bar{\mathbf{n}}^j$, defined in body $j$ coordinate system, can be written as $\delta = (\mathbf{R}^i + \mathbf{A}^i\bar{\mathbf{u}}^i - \mathbf{R}^j - \mathbf{A}^j\bar{\mathbf{u}}^j) \cdot \left(\mathbf{A}^j\bar{\mathbf{n}}^j\right)$, where $\mathbf{R}^i$ and $\mathbf{R}^j$ are the global positions of the centers of mass of the two components, $\bar{\mathbf{u}}^i$ and $\bar{\mathbf{u}}^j$ are the local position vectors of the two contact points with respect to their component center of mass, and $\mathbf{A}^i$ and $\mathbf{A}^j$ are the rotation matrices that define the orientations of the component coordinate systems. The vector of relative velocity at the contact point can be written as $\mathbf{v}_r^{ij} = \dot{\mathbf{R}}^i + \boldsymbol{\omega}^i \times \left(\mathbf{A}^i\bar{\mathbf{u}}^i\right) - \dot{\mathbf{R}}^j - \boldsymbol{\omega}^j \times \left(\mathbf{A}^j\bar{\mathbf{u}}^j\right)$, where $\boldsymbol{\omega}^i$ and $\boldsymbol{\omega}^j$ are the absolute angular velocity vectors of the two bodies. Using the penetration and the vector of relative velocity, the normal component of the contact force can be defined as $f_n = k\delta + c_n\left(\mathbf{v}_r^{ij} \cdot \mathbf{n}^j\right)$, where $\mathbf{n}^j = \mathbf{A}^j\bar{\mathbf{n}}^j$, and $k$ and $c_n$ are assumed stiffness and damping coefficients. In the numerical study performed in this investigation, the stiffness and damping coefficients are assumed $k = 1 \times 10^6$ N/m and $c_n = 1 \times 10^3$ N·s/m, respectively. Using the normal force, the tangential friction force can be computed using the coefficient of dry friction $\mu$ as $f_t = \mu f_n$. In this study the coefficient of dry friction $\mu$ is assumed 0.5. This tangential force acts in a direction opposite to the direction of the relative velocity between the two contact surfaces.

### 8.6 Modeling assumptions

In the bogie models considered in this study, the car body weight is not considered to focus the attention on the bogie performance. Because the axle loads for these bogies are different, more investigations are needed in the future to have better understanding of the bogie behavior when used to support laden rail cars. Because actual bogie designs may include more springs in the suspension, the reduced number of springs used in the models considered in this investigation represent equivalent spring systems. Furthermore, the stiffness coefficients of the springs are assumed constant for simplicity despite the fact that the actual springs can have nonlinear characteristics which are not available to the authors. Use of linear spring models can be justified in the case of small spring deflections. According to the BS EN 16,235:2013 standard, the suggested stiffness of vertical tare springs is around $1.2 \times 10^6$ N/m for the Y25 bogie. However, a stiffness of $1.69 \times 10^6$ N/m is adopted to be consistent with the spring coefficient used for the three-piece bogie to have a more meaningful comparison between the two designs.

In the Y25 bogie design, the longitudinal motion of axle boxes is restricted to a stroke of few millimeters by limiting the yaw oscillations of the wheelsets. Such a restriction is not considered in this investigation since axle box displacements are small because the curve used is not very tight.

## 9 Numerical results

Numerical results of the MBS dynamic simulations of the three-piece and Y25 bogies are presented in this Section. The results are obtained by considering only the individual bogies without the rail car in order to have clear understanding of the bogie behavior without considering other loading conditions that can influence the motion characteristics. More focused investigations are needed to understand the effect of heavier axle loads on the bogie performance. Because of the large number of design variants of each bogie type and the difficulties of obtaining exact inertia, dimension, and suspension data, the results are presented in this Section without making an overall judgment on the bogie performance.

### 9.1 Angle of attack

The angle of attack is computed and plotted for the front and the rear wheelsets of each bogie, as shown in Figs. 13 and 14. Figure 13 presents the results that compare the angle of attack for the front wheelset, while Fig. 14 shows the comparison for the rear wheelset. The results presented in these two Figures show, as expected, that the leading wheelset has more variations in the angle of attack as compared to the rear wheelset. Also, as expected, spikes in the angle of attack are observed at the points of transition between different track segments. The non-zero values of the angle of attack shown in these Figures do not always imply wheel flange/rail contact. The results show that the angle of attack oscillates around zero along the tangent segments,

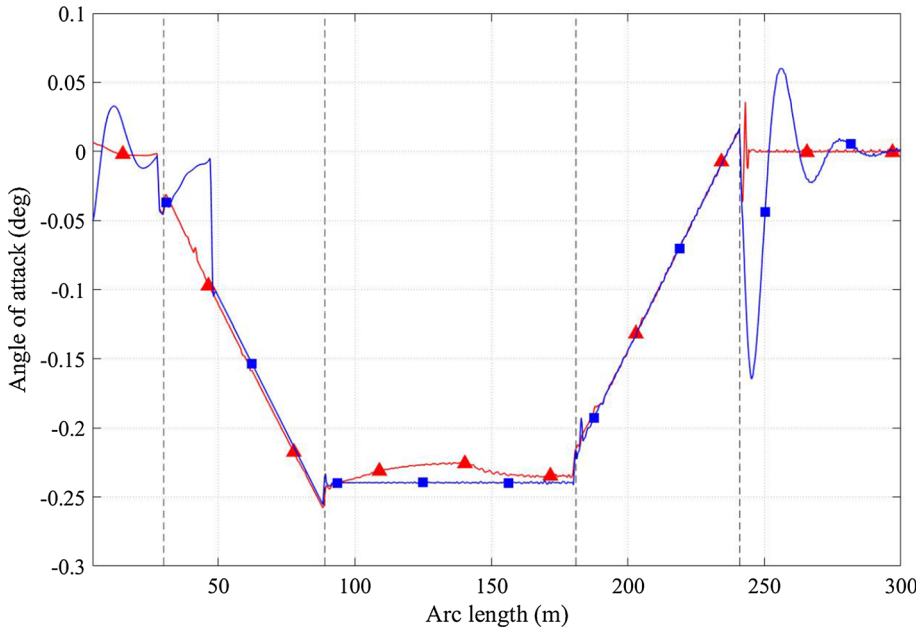


**Fig. 13** Angle of attack of the leading wheelset (Three-piece bogie, Y25 bogie)

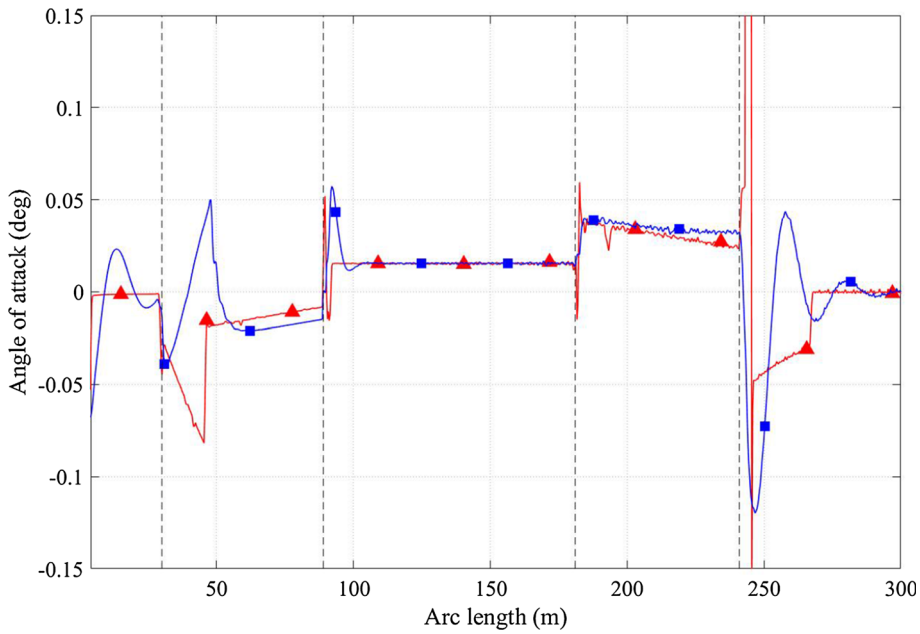


**Fig. 14** Angle of attack of the rear wheelset (Three-piece bogie, Y25 bogie)

while it takes a rather constant nonzero value along the curve, indicating a wheel flange/rail contact during the curve negotiation. The motion on the first and second spiral segments is characterized by a near linear variation of the angle of attack. This implies, as expected, that deviation of the wheelset from the track orientation starts increasing at the beginning of the spiral segments and reaches a stable value during the curve, a trend confirmed by results presented in previous investigations [19].

By comparing the results of the two bogies, it can be seen that the angle of attack of the Y25 bogie front wheelset has larger perturbations at the track transitions as compared to the three-piece bogie, particularly at the intersection between the curve and the second spiral segment. However, at the same point, a large spike in the angle of attack of the rear wheelset of the three-piece bogie can also be observed. The largest value of the

angle of attack observed in the simulations was found to be 1.4°. Based on the results obtained in this study, the leading wheelset seems to have smaller angle of attack in the three-piece bogie, while the rear wheelset of the Y25 bogie has a smaller angle of attack.

### 9.2 Flange contact forces

Figures 15 and 16 show the flange contact forces that arise during simulations of the three-piece and Y25 bogies. The results presented in these Figures can be used to explain the problems associated with the lateral force balance currently used in practice to determine the balance speed. It can be observed from the results presented in Figs. 15 and 16 that the front wheelset of the three-piece bogie has a flange contact only during the second spiral segment, while the left rear wheelset flange maintains contact with large section of the first spiral segment and along the entire curve. A similar behavior is observed for the front wheelset of the Y25 bogie, which is the only wheelset that experiences flange contact for this bogie model. Because simulations are performed at the balance speed, if the equilibrium condition between the lateral component of the centrifugal inertia and gravity forces were achieved, wheel/rail contacts could be avoided during the curve negotiation. In view of these results, the performance of the leading wheelset of the three-piece bogie is better compared to the Y25 bogie. However, the rear wheelset of the Y25 bogie appears to smoothly follow the track, a behavior which is not observed for the three-piece bogie.

### 9.3 Centrifugal force

The centrifugal forces of the bogie components can be evaluated using motion trajectories predicted using the MBS simulations as previously discussed in this paper. To have a more useful representation of the centrifugal force for the multi-component bogies, one can compute the vector sum of all centrifugal forces of the components based on their actual motion trajectories predicted using the DDS approach described in this paper. Using this approach, the total sum of the centrifugal forces can be determined, but the resultant vector is not associated with a particular point of application on a particular bogie component. Furthermore, the distances between the mass centers of individual components lead to moments that are not considered using this approach. For these reasons, the result of the force sum adopted in this paper serves as an index of the centrifugal force magnitude rather than an actual centrifugal force measure. The simulation-based motion trajectory results are compared with the results based on the lateral track plane force equilibrium used in practice to determine the balance speed based on the track geometry instead of the recorded motion trajectories. Figures 17 and

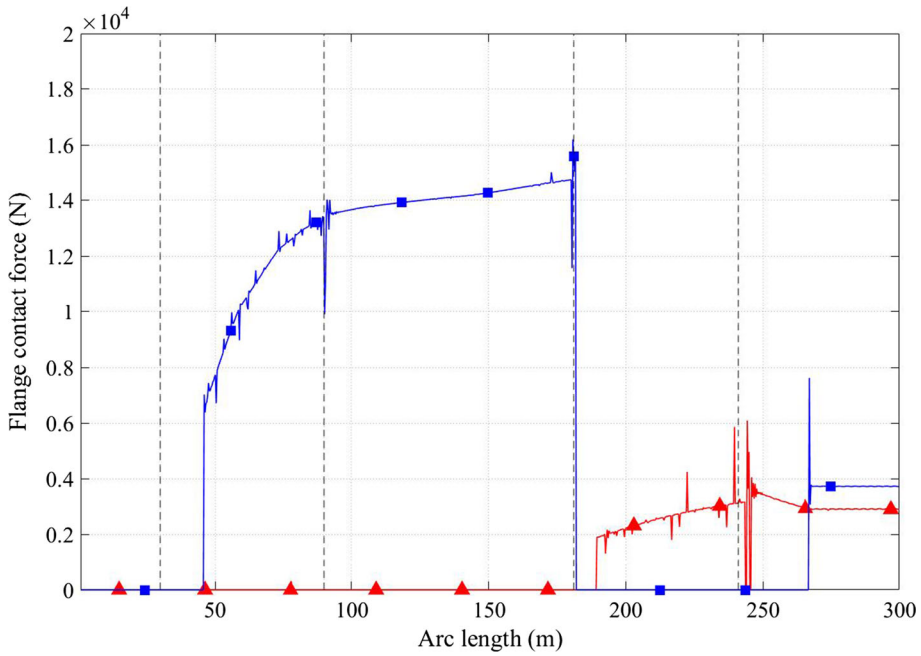


**Fig. 15** Flange contact forces of the three-piece bogie (—▲— Front right contact, —■— Left rear contact)

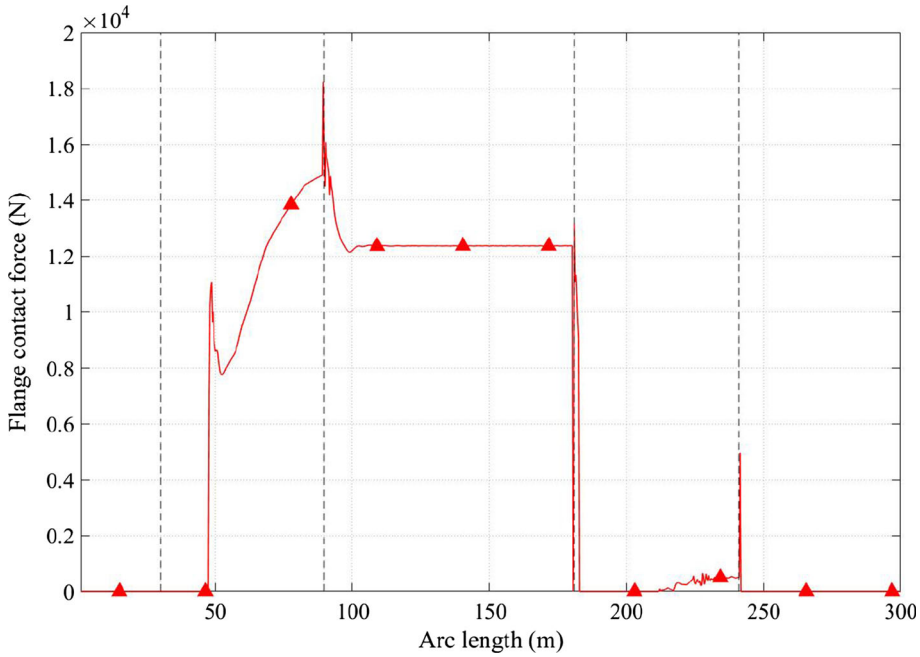


**Fig. 16** Flange-contact forces of the Y25 bogie (—▲— Front right contact)

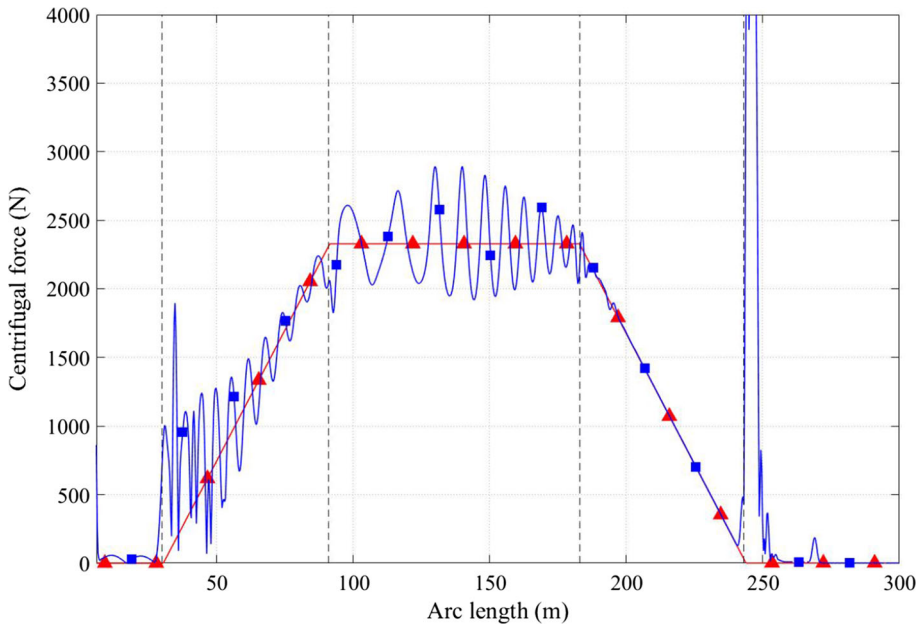


**Fig. 17** Centrifugal force magnitude of the three-piece bogie (—▲— Track geometry, —■— Motion trajectories)

18 show the difference between the two methods used for computing the centrifugal forces. In case of the three-piece bogie, the magnitude of the centrifugal force appears to be more oscillatory, and the force spike at the end of the second spiral reaches 7700 N. On the other hand, the magnitude of the centrifugal force of the Y25 bogie follows the expected trend, with small perturbations only at the track transitions. Therefore, the trajectory traced by the Y25 bogie is more likely to have less deviations from the track centerline.

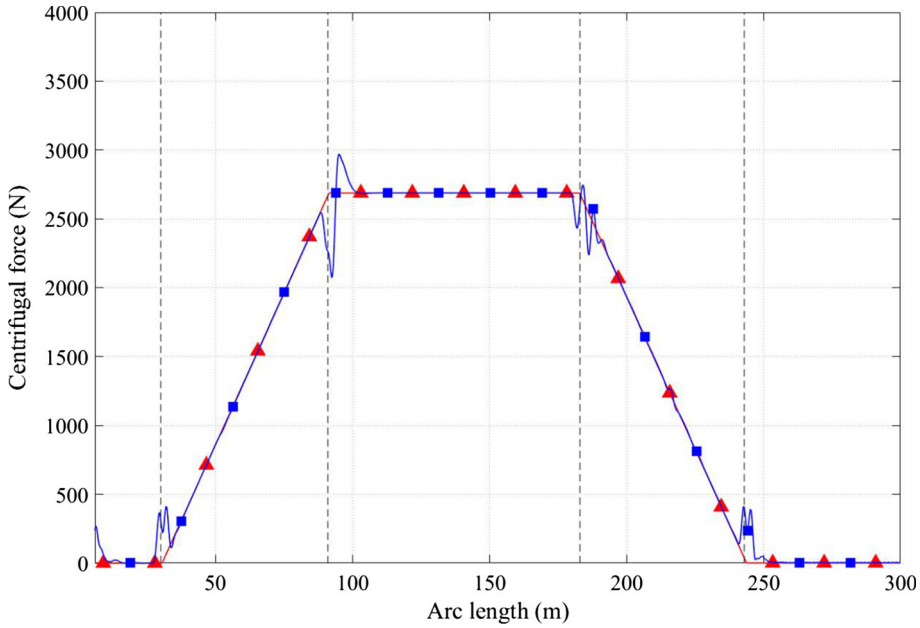


**Fig. 18** Centrifugal force magnitude of the Y25 bogie (—▲— Track geometry, —■— Motion trajectories)

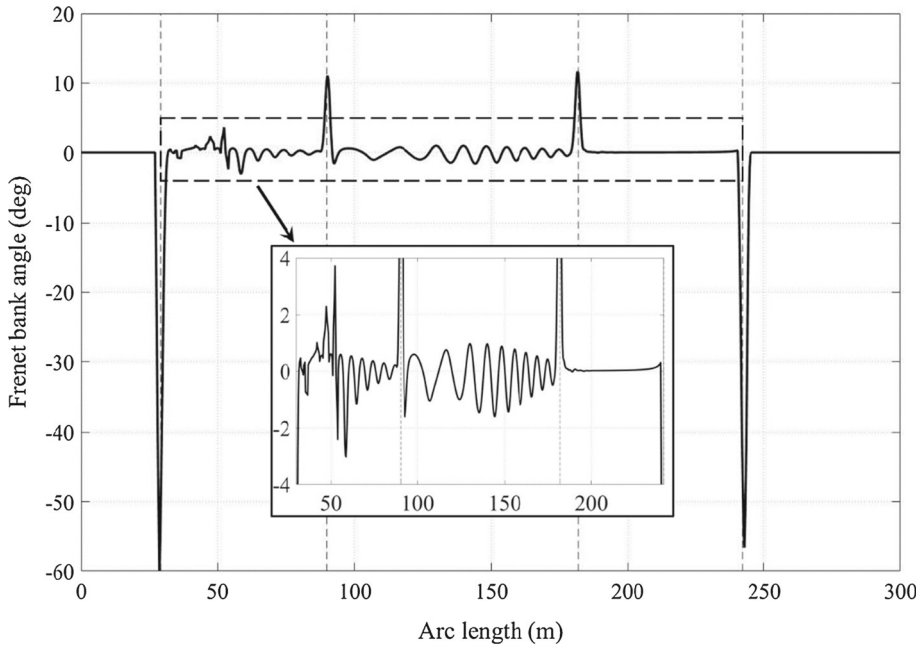


**Fig. 19** Frenet bank angle of the front wheelset of the three-piece bogie

## 9.4 Frenet bank angle

Figures 19, 20, 21, and 22 show the Frenet bank angle computed for the wheelsets of the three-piece and Y25 bogies using the recorded motion trajectories. The results are compared with the motion-independent track bank angle used in practice. The Frenet bank angle defines the super-elevation of the motion plane, while the track bank angle defines the super-elevation of the track plane. Since the centrifugal force acts in the direction of the curve normal vector, which lies in the motion plane, a non-zero Frenet bank angle indicates violation of the assumption of horizontal centrifugal force used in practice to define the balance speed.

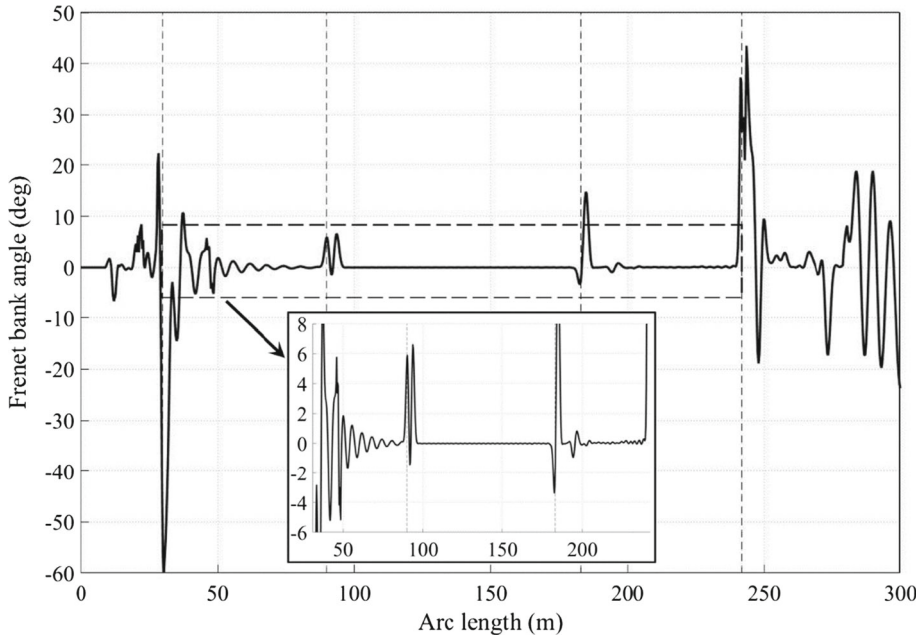


**Fig. 20** Frenet bank angle of the rear wheelset of the three-piece bogie

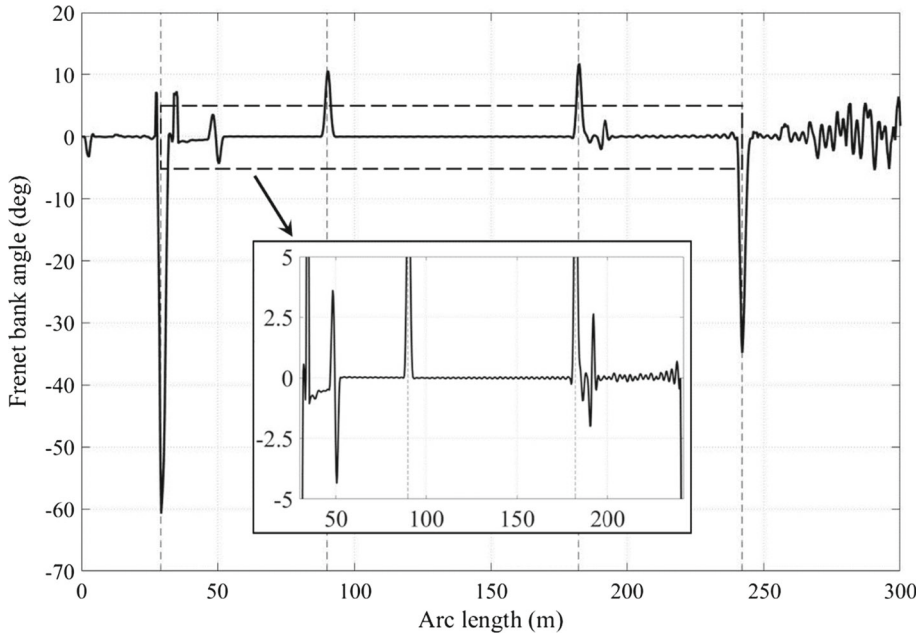


**Fig. 21** Frenet bank angle of the front wheelset of the Y25 bogie

Along the tangent segments, even if the lateral and vertical deviations of the motion trajectory from the track centerline are small, the Frenet bank angle appears to be sensitive to the change of the curvature of the motion trajectory curves which can represent very tight curves. Near the start of the first spiral and end of the second spiral, spikes due to the track transitions can be observed for all wheelsets, particularly the rear ones. When the Frenet bank angle is zero, the centrifugal force lies in a plane parallel to the horizontal plane, which is the assumption currently made in defining the balance speed. It is important to notice, from the results presented in Figs. 19, 20, 21, and 22, that this condition is only met in case of flange contacts, a situation which is not desirable because of the forces exerted on the vehicle and the track structure that can lead to significant wear or possibly derailments. The wheel/rail flange contact is a clear indication that the track plane lateral

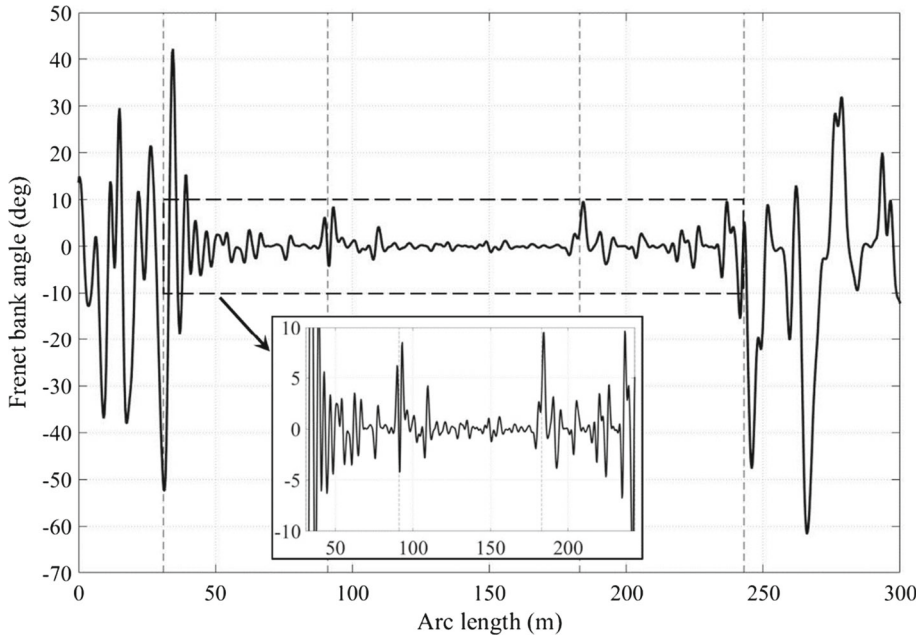


**Fig. 22** Frenet bank angle of the rear wheelset of the Y25 bogie

force equilibrium used in practice to define the balance speed is violated and does not prevent the vehicle from sliding toward the high or low rail. The results presented in Figs. 19, 20, 21, and 22 show that the Frenet bank angle has more oscillations for the three-piece-bogie front wheelset and for the Y25 bogie rear wheelset. Larger Frenet bank angle can imply higher level of force self-balancing by the component of the gravity force in the osculating plane.

## 10 Summary and conclusions

A new *Frenet force analysis* integrated with a *data-driven science* (DDS) approach is proposed for the evaluation of railroad vehicle performance. Use of the new performance evaluation methodology, which is based on integrating nonlinear *multibody system* (MBS) computational algorithms and new geometric concepts, is demonstrated by comparing the performance of two widely used railroad bogies: the *three-piece bogie*, used in North America and other parts of the world, and the European *Y25 bogie*. Despite their wide use, a MBS comparative study based on Frenet force analysis is lacking in the literature. In this investigation, distinction is made between AMT curves and the track geometries. The AMT curve geometry is defined using the motion-dependent Frenet curvature, and vertical-development angles, which differ from their motion-independent counterparts used in the description of the track geometry. Furthermore, distinction is made between the Frenet super-elevation defined by the Frenet bank angle of AMT curves and the motion-independent track super-elevation defined by the track bank angle. The difference between the *lateral track plane force balance* used in practice to determine the balance speed and the *Frenet force balance* based on recorded motion trajectories is explained. Computer simulations of bogies travelling on a track, consisting of tangent, spiral, and curve sections, are performed, and the results obtained demonstrated the dependence of the AMT curve geometry on the wheelset forward motion, highlighting the limitations of tests performed using roller test rigs which do not allow longitudinal wheelset motion.

While a judgment on the overall bogie performance cannot be made based on the results of a single investigation, the results obtained show that flange contacts occur for both the three-piece-bogie wheelsets and only for the Y25 bogie front wheelset, despite performing the simulations at the balance speed. This demonstrates that the current balance speed, while it lowers the impact severity, is not effective in totally eliminating the flange contact during curve negotiations. In general, the three-piece-bogie front wheelset shows more stable behavior compared to the rear wheelset, while the opposite is observed for the Y25 bogie. The tendency of the Y25 bogie rear wheelset to follow the track is probably attributed to the high rigidity of the bogie frame. The flange contact force results indicate that the three-piece-bogie wheels may be subjected

to more flange wear due to the two-point contacts occurring for both wheelsets. It is important, however, to point out that previous investigations reported that the performance of the three-piece bogie can be worsened in the unloaded conditions [30, 38]. Because all bogie performance criteria cannot be addressed in a single investigation and because of the lack of exact inertia, dimension, and material data, this study was focused on specific measures without making judgment on the overall bogie performance.

**Acknowledgements** This research was supported by the National Science Foundation (Project # 1632302).

## References

1. Andersson, C., Abrahamsson, T.: Simulation of Interaction between a train in general motion and a track. Veh. Syst. Dyn. **38**(6), 433–455 (2002)
2. Berghuvud, A.: Freight car curving performance in braked conditions. IMechE J. Rail Rapid Transit **216**(1), 23–29 (2002)
3. Bosso, N., Gugliotta, A., Somà, A.: Multibody simulation of a freight bogie with friction dampers. ASME/IEEE Joint Rail Conf. **35936**, 47–56 (2002)
4. Cuenot, F., Gabriel, C.H.: Carbon Footprint of Railway Infrastructure. In: International Union of Railways (2016)
5. De Pater, A.D.: The geometrical contact between track and wheelset. Veh. Syst. Dyn. **17**(3), 127–140 (1988)
6. Do Carmo, M.P.: Differential Geometry of Curves and Surfaces, 2nd edn. Dover Publications, New York (2016)
7. Dumitriu, M.: The stationary motion of a bogie along a circular curve. UPB Sci. Bull. Ser. D **74**, 39–50 (2012)
8. Elkins, J.A., Gostling, R.J.: A general quasi-static curving theory for railway vehicles. Veh. Syst. Dyn. **6**(2–3), 100–106 (1977)
9. Endlicher, K.O., Lugner, P.: Computer simulation of the dynamical curving behavior of a railway bogie. Veh. Syst. Dyn. **19**(2), 71–95 (1990)
10. Farin, G.: Curves and Surfaces for CAGD, A Practical Guide, 5th edn. Morgan Kaufmann, Publishers, San Francisco (1999)
11. Gallier, J.: Geometric Methods and Applications: For Computer Science and Engineering. Springer, New York (2011)
12. Ghazavi, M.R., Taki, M.: Dynamic simulations of the freight three-piece bogie motion in curve. Veh. Syst. Dyn. **46**(10), 955–973 (2008)
13. Ginsberg, J.: Engineering Dynamics. Cambridge University Press, New York (2008)
14. Goetz, A.: Introduction to Differential Geometry. Addison Wesley, London (1970)
15. Goldstein, H.: Classical Mechanics. Addison-Wesley, London (1950)
16. Grassie, S.L.: Dynamic modeling of the track and their uses. In: Kalker, J.J., Cannon, D.F., Orringer, O. (eds.) Rail Quality and Maintenance for Modern Railway Operation, pp. 165–184. Kluwer, Dordrecht (1993)
17. Greenwood, D.T.: Principles of Dynamics, 2nd edn. Prentice Hall, Englewood Cliffs (1988)
18. Handoko, Y., Xia, F., Dhanasekar, M.: Effect of asymmetric brake shoe force application on wagon curving performance. Veh. Syst. Dyn. Dyn. **41**, 113–122 (2004)
19. He, Y., Mcphee, J.: Optimization of curving performance of rail vehicles. Veh. Syst. Dyn. **43**(12), 895–923 (2005)
20. Huston, R.L.: Multibody Dynamics. Butterworth-Heinemann, Stoneham (1990)
21. Hecht, M.: European freight vehicle running gear: today's position and future demands. Proc. Inst. Mech. Eng. Part F J. Rail Rapid Transit **215**(1), 1–11 (2001)
22. Iwnicki, S.D., Stichel, S., Orlova, A., Hecht, M.: Dynamics of railway freight vehicles. Veh. Syst. Dyn. **53**(7), 995–1033 (2015)
23. Jalili, M.M., Motavasselolhagh, M., Fatehi, R., Sefid, M.: Investigation of sloshing effects on lateral stability of tank vehicles during turning maneuver. Mech. Based Des. Struct. Mach. (2020). https://doi.org/10.1080/15397734.2020.1800490
24. Jönsson, P.A.: Dynamic Vehicle-Track Interaction of European Standard Freight Wagons with Link Suspension. Doctoral dissertation, KTH (2007)
25. Kataori, A., Iijima, H., Momosaki, S., Horioka, K.: Development of continuous measurement equipment for angle of attack and results of measurements. JR East Tech. Rev. **19**, 46–49 (2011)
26. Kik, W.: Comparison of the behavior of different wheelset-track models. Veh. Syst. Dyn. **20**(1), 325–339 (1992)
27. Knothe, K.L., Grassie, S.L.: Modeling of railway track and vehicle/track interaction at high frequencies. Veh. Syst. Dyn. **22**(3–4), 209–262 (1993)
28. Knothe, K., Stichel, S.: Direct covariance analysis for the calculation of creepages and creep-forces for various bogie on straight track with random irregularities. Veh. Syst. Dyn. **23**(1), 237–251 (1994)
29. Kreyszig, E.: Differential Geometry. Dover Publications, London (1991)
30. Kovalev, R., Lysikov, N., Mikheev, G., Pogorelov, D., Simonov, V., Yazykov, V., Torskaya, E.: Freight car models and their computer-aided dynamic analysis. Multibody Sys. Dyn. **22**(4), 399–423 (2009)
31. Ling, H., Shabana, A.A.: Euler angles and numerical representation of the railroad track geometry. Acta Mech. (2021, in press)
32. Pascal, J.P., Sany, J.R.: Dynamics of an isolated railway wheelset with conformal wheel-rail interactions. Veh. Syst. Dyn. **57**(12), 1947–1969 (2019)
33. Piegl, L., Tiller, W.: The NURBS Book, 2nd edn. Springer, Berlin (1997)
34. Rail Safety and Standards Board: Railway Wheelsets. Rail Safety and Standards Board Limited (2017)
35. Railway Technical: Vehicle Suspension Systems. http://www.railway-technical.com/archive/vehicle-suspension-systems.pdf (2004). Accessed 02 April 2021
36. Rogers, D.F.: An Introduction to NURBS with Historical Perspective. Academic Press, San Diego (2001)
37. Roberson, R.E., Schwertassek, R.: Dynamics of Multibody Systems. Springer, Berlin (1988)

38. Sadeghi, M., Shadfar, M., Rezvan, M.: Dynamic modeling of three pieces bogies at curves and the parameters affecting its derailment index. In: International Heavy Haul Association Conference (2011)
39. Shabana, A.A.: Dynamics of Multibody Systems, 5th edn. Cambridge University Press, New York (2020)
40. Shabana, A.A.: Mathematical Foundation of Railroad Vehicle Systems: Geometry and Mechanics. Wiley, London (2021)
41. Shabana, A.A.: Frenet Oscillations and Frenet-Euler Angles: Curvature Singularity and Motion-Trajectory Analysis. Nonlinear Dynamics (2021, in press)
42. Shabana, A.A.: Geometric self-centering and force self-balancing of railroad vehicle hunting oscillations. Acta Mech. (2021, in press)
43. Shabana, A.A., Ling, H.: Characterization and quantification of railroad spiral-joint discontinuities. Mech. Based Des. Struct. Mach. **6**, 1–26 (2021)
44. SKF: Railway Technical Handbook Vol. 1: Axleboxes, wheelset bearings, sensors, condition monitoring, subsystems and services. In: SKF, Göteborg (2011)
45. Sun, Y.Q., Cole, C.: Vertical dynamic behavior of three-piece bogie suspensions with two types of friction wedge. Multibody Syst. Dyn. **19**(4), 365–382 (2008)
46. Technical Specialist Rolling Stock Performance Standards: ESR 0331. Wheel and axles reference manual. RailCorp Engineering Standard (2013)
47. The American Public Transportation Association: APTA PR-M-S-015-06 Standard for Wheel Flange Angle for Passenger Equipment. APTA PRESS Task Force (2007)
48. The Contact Patch: https://the-contact-patch.com/book/rail. (2017). Accessed 03 Jan 2021
49. True, H.: Does a critical speed for railroad vehicles exist? In: Proceedings of IEEE/ASME Joint Railroad Conference, pp. 125–131 (1994)